Development of metal-organic framework-based catalysts for enhanced aqueous nitrate removal

Miriam Absalyamova, B.Eng. in Chemical Engineering

submitted in fulfillment of the requirements for the degree of Master of Science in Chemical and Materials Engineering

School of Engineering and Digital Sciences
Department of Chemical and Materials Engineering
Nazarbayev University

53 Kabanbay Batyr Avenue,
Astana, Kazakhstan, 010000
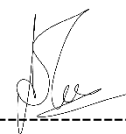
Supervisor: Professor Stavros Poulopoulos

Co-supervisor: Professor Woojin Lee

April 2023

DECLARATION

I hereby declare that this manuscript, entitled "*Development of metal-organic framework-based catalysts for enhanced aqueous nitrate removal*" is the result of my own work except for quotations and citations which have been duly acknowledged.

I also declare that, to the best of my knowledge and belief, it has not been previously or concurrently submitted, in whole or in part, for any other degree or diploma at Nazarbayev University or any other national or international institution.

Name: Miriam Absalyamova

Date: 07.04.2023

Abstract

This thesis focuses on the development of a catalyst supported by the metal-organic framework (MOF)-derived Co-doped material for the reduction of nitrate (NO_3^-) in aqueous systems. Nitrate pollution poses severe risks to human health and the environment, and efficient technologies are required for its control. The catalytic reduction of aqueous nitrate is a desirable choice since it can be tailored to the necessary reactivity and selectivity and requires no excessive energy inputs. The study aims to synthesize and characterize zeolitic imidazole framework ZIF-67-based catalysts and evaluate the catalytic activity for nitrate removal in batch kinetic tests. The study also aims to investigate different parameters affecting the reactivity and selectivity of the process to achieve the optimum conditions, identify the reaction mechanism by analytical investigation of the catalyst surface before and after reaction, and evaluate the catalyst stability and durability in consecutive reaction cycles with analysis of metal leaching.

Compared to other catalysts reported in the literature, Pt-Co@NC showed competitiveness, demonstrating one of the highest rate constants for the reaction at similar conditions. Carbonization of ZIF-67 resulted in the improved stability of the structure, exposing Co to the surface of carbon material. Impregnation of Pt on the surface of Co@NC was beneficial for nitrate reduction compared to other metals and resulted in enhanced reactivity with the full reduction of 60 mg/L NO_3^- -N in 30 min. Moreover, an increase in catalyst loading and Pt content positively affected the reactivity of the system as well as the reduction in contaminant concentration.

Overall, the study's findings suggest that Pt-Co@NC can effectively reduce nitrate pollution in aqueous systems with high selectivity towards ammonium (NH_4^+). The catalyst is durable and stable, making it a promising candidate for nitrate removal from water sources. The study provides valuable insights into the synthesis and characterization of ZIF-based catalysts and their catalytic activity for nitrate removal.

Acknowledgments

I would like to express my gratitude to the following individuals and organizations who have contributed to the successful completion of this Master's thesis.

Firstly, I would like to thank Professor Poulopoulos and Professor Lee for their valuable guidance, insightful feedback, and endless support throughout the thesis writing process. Being a part of Professor Lee's research group was an honor that brought an unforgettable experience and raised me as a young scientist. Thanks to Professor Sungjun Bae and his students for the warm welcome and assistance with material characterization during my short visit to Konkuk University.

I am grateful to my friends and colleagues from GEERG for making these two years of graduate school enjoyable and fun. Special thanks to my family and close ones for being by my side and supporting me throughout my studies.

Table of content

List of Abbreviations & Symbols

2-MIM	2-methylimidazole
Co@NC	Co-doped N-codoped carbon
DDIW	Deaerated deionized water
DI	Deionized water
EDS	Energy dispersive X-ray spectroscopy
FESEM	Field Emission Scanning Electron Microscopy
FTIR	Fourier Transformed Infrared spectroscopy
IC	Ion chromatography
ICP-MS	Inductively coupled plasma mass spectrometry
ICP-OES	Inductively Coupled Plasma Optical Emission spectroscopy
IR	Infra-red
M_n	Noble metal
MOF	Metal-organic framework
M_p	Promoter metal
NC	N-doped carbon
NH_4^+-N	Ammonium nitrogen
NO_2^--N	Nitrite nitrogen
NO_3^--N	Nitrate nitrogen
pH_{PZC}	Point of zero charge
$R_{NO_3^-}$	NO3- removal efficiency
RO	Reverse Osmosis
$S_{NO_2^-}$	Selectivity
SEM	Scanning electron microscope
STA	Simultaneous Thermal Analyzer
TEM	Transmission electron microscope
TGA	Thermogravimetric analysis
WHO	World Health Organization
XPS	X-ray photo-electron spectroscope
XRD	X-ray diffraction
ZIF	Zeolitic imidazolate framework
ZVA	Zero valent aluminum
ZVC	Zero valent copper
ZVI	Zero valent iron
ZVM	Zero valent magnesium
ZVZ	Zero valent zinc

List of Tables & Figures

Chapter 1 - Introduction

Nitrate (NO$_3^-$), one of the main groundwater pollutants, contaminates water sources from extensively fertilized soil, landfills, urban drainage, and septic systems [1]. At increased concentrations, NO$_3^-$ severely risks human health and the environment. The nitrate's toxicity mainly comes from its reduced form, nitrite (NO$_2^-$). These nitrogen species in aqueous sources are of high concern for pregnant women and infants' health due to the risk of methemoglobinemia, or a "blue baby syndrome," occurring because nitrite binds more strongly to hemoglobin than oxygen [2]. Nitrite pollution relation also to an elevated risk of gastric cancer. Water quality standards and norms in the Republic of Kazakhstan classify nitrate as a "dangerous" pollutant, while nitrite is "highly dangerous" [3]. Regulations set nitrate and nitrite concentration limits of 45 mg/L and 3.3 mg/L in water sources for domestic use [3], [4]. World Health Organization (WHO) standards set the limit of 50 mg/L of nitrate in water reservoirs [5]. Developing efficient technologies to control nitrogen species concentration in an aqueous environment of essential need.

Although the adequate use of nitrogen fertilizers is needed to reduce nitrate pollution, several methods are adopted for nitrate removal from water sources, including ion exchange, reverse osmosis, and biological denitrification [6]. They all produce secondary waste of high contaminant concentration and require frequent media regeneration. The most popular method, biological denitrification, is efficient but requires intense maintenance and a steady supply of organic substrates. Additionally, waste sludge is created during the process, and constant temperature control is required to maintain high levels of reactivity. Since it produces no secondary waste and can be tailored to the necessary reactivity and selectivity, enhanced catalytic reduction of nitrates is a desirable choice. In the current work, the chemical reduction of aqueous nitrate with the help of a catalyst will be investigated. There are numerous different catalyst systems were suggested for NO$_3^-$ removal, including zeolites, zero-valent iron, and Fe-containing minerals [7], [8]. Nitrate reduction path could produce ammonium ($NO_3^- \rightarrow NO_2^- \rightarrow NO \rightarrow NH_2OH \rightarrow NH_4^+$) or nitrogen gas ($NO_3^- \rightarrow NO_2^- \rightarrow NO \rightarrow N_2O \rightarrow N_2$). Metal-organic framework (MOF) materials could suggest numerous beneficial properties for the use in catalytic systems [8].

This work aims to study the reduction of NO$_3^-$ in aqueous systems by bimetallic catalysts supported by MOF-derived Co-doped material. The following experimental tasks were addressed to reach the established aim: (**1**) synthesis and characterization of zeolitic imidazole framework (ZIF)-based catalysts; (**2**) evaluation of catalytic activity of ZIF-derived catalyst for nitrate removal catalyst

in batch kinetic tests; **(3)** selection and variation of different parameters affecting the reactivity and selectivity of the process to achieve the optimum conditions; **(4)** investigation of catalyst surface after reaction by analytical methods; **(5)** evaluation of catalyst stability and durability in consecutive reaction cycles.

The following thesis comprises five chapters: 1) Introduction, 2) Literature review, 3) Materials and methods, 4) Results and discussion, 5) Conclusion.

Chapter 2 - Literature review

The literature review focuses on sources of nitrate pollution and ways to remove it from the aqueous environment. Catalytic nitrate reduction methods and description of metal-organic framework applications are represented in the following subsections as well.

2.1. Aqueous nitrate pollution

Nitrate is an integral part of nitrogen cycles and plays a vital role in the functioning of all biological species. Nitrogen is essential to plant growth, and it should be available in inorganic form as ammonia (NH_3), ammonium (NH_4^+), nitrite (NO_2^-), or nitrate (NO_3^-). Soil microorganisms break down organic compounds, releasing inorganic nitrogen [9]. In terrestrial ecosystems, nitrogen can be found as dead organic matter; however, the sources of naturally occurring nitrogen gradually decrease due to deforestation and anthropogenic activities. Meanwhile, the increased need for food supply due to the growing human population and the depletion of soil resources stimulates the extensive use of inorganic fertilizers.

Fertilizers are an integrated part of the world's agricultural sector development as they provide essential elements for enhanced growth of crops and blossoming harvests. The constant growth of the world population and high demand for food across the globe leads to a higher reliance on inorganic and organic fertilizers [10]. The Food and Agriculture Organization of the United Nations reported that nitrogen consumption in 2014 increased by 32.2% compared to 2000 [11]. It is estimated that nitrogen consumption will increase by 172% by 2050. In Kazakhstan, fertilizers are paramount due to the soil quality and high demand for agricultural products. 190 thousand tons of ammonium nitrate was purchased by Kazakhstani farmers in 2020 [12]. Moreover, the largest supplier produced 380 711 tons of nitrogen fertilizers in 2021. Extensive consumption of fertilizers leads to excessively concentrated amounts of nitrate in the soil, which then leaks into groundwater and deteriorates the quality of the soil and water bodies [13]. It has been reported that only half of the supplied nitrogenous fertilizers are used by plants, while the rest either evaporates, reacts with organic compounds, or leaks into the groundwater. The latter accounts for approximately 2-10% of the total nitrogen supplied with fertilizers [10]. Highly mobile and water soluble NO_3^- species can easily spread to large distances and enter surface water and groundwater. While one of the most efficient ways to reduce the nitrogen input into ecosystems is to limit the use of agricultural fertilizers, emergent actions should be taken

for the treatment of the nitrite-polluted environment to provide fresh water and control the growth of microorganisms in water bodies. About 20% of European groundwater bodies are contaminated with nitrates, mainly due to agricultural activities, according to a report by the European Environment Agency (EEA). In addition to agricultural activities, anthropogenic nitrogen sources include manure pools, septic and sewer system leakage, and the discharge of untreated industrial and domestic wastewater [6].

At increased concentrations, NO_3^- severely threatens human health and the environment. Nitrate toxicity is mainly due to its reduced form, nitrite (NO_2^-). These nitrogen species in aqueous sources are of great concern for pregnant women and infants' health due to the risk of methemoglobinemia, or a 'blue baby syndrome', a medical condition when blood loses the ability to carry oxygen to the tissues [5]. Nitrate pollution has also been linked to various health problems, including cancer and reproductive issues [5]. Besides human health risks, an elevated concentration of NO_3^- in poorly buffered freshwater leads to eutrophication disrupting normal ecosystems of rivers and lakes [2], [14]. Water quality standards and norms in the Republic of Kazakhstan classify nitrate as a "dangerous" pollutant, while nitrites are "highly dangerous" [3]. Regulations set nitrate and nitrite concentration limits of 45 mg/L and 3.3 mg/L in water sources for domestic use. World Health Organization (WHO) uses the limit of 50 ppm for NO_3^- concentrations in water to reduce health risks related to nitrate consumption [5]. Developing efficient technologies to control the concentration of nitrogen species in an aqueous environment of essential need.

2.2. Technologies for the removal of nitrate from water

Various methods have been incorporated for the treatment of nitrate-polluted water. Nitrates are removed through various technologies, divided into two main categories: nondestructive and destructive methods [6]. Non-destructive methods include the removal of NO_3^- by ion exchange, adsorption, and reverse and forward osmosis techniques.

Ion exchange is a chemical process in which ions of a given type (e.g., cations or anions) are exchanged with ions of the same charge that are bound to a solid matrix, usually a resin or a gel [15]. This exchange occurs due to electrostatic interactions between the mobile ions in the solution and the oppositely charged functional groups on the solid matrix. During treatment, nitrate and other anions in water are exchanged with chloride in the resin, thus releasing chloride into the water [16]. Then the resin is regenerated with sodium chloride solution (brine) and the exchange process is reversed. This

technology is used in small or medium size water treatment plants and has advantages of process control and easiness of operation. However, while ion exchange can be effective for removing nitrates from wastewater, it may not be the best option for all situations and can have some significant drawbacks that need to be considered [16]. These include expensive operation due to exchange resins cost, need for regular regeneration and, most importantly from environmental point of view, regeneration of the exchange resin can generate large volumes of waste, which may require additional treatment and disposal [15], [16].

The adsorption process involves the attachment of nitrate molecules to the surface of the adsorbent material, which can then be removed from the water [17]. Activated carbon is an effective adsorbent for nitrate removal due to its large surface area and high porosity [17], [18]. Zhou et al. developed FeMgMn layered double hydroxide with capacity of 10.56 N-mg/g and removal rate of 86.26% with the adsorbent dose of 5 g/L in real water [19]. While adsorption methods are effective in removing nitrate from water, there are also some disadvantages to using adsorbents for this purpose. One major drawback is that the adsorbents become saturated with nitrate over time, reducing their effectiveness and requiring replacement and regeneration [18], [20]. Additionally, the process of regeneration can be costly and may require the use of chemicals or energy. Finally, the initial cost of setting up an adsorption system can be high, and ongoing maintenance costs may also be a consideration [20].

In reverse osmosis (RO), water is forced through a semi-permeable membrane under high pressure, which allows for the removal of dissolved solids, including nitrate [21]. Nitrate is removed by electrostatic interaction and size exclusion on the membrane surface [22]. RO has several advantages, including high efficiency, low energy consumption, and the ability to remove a wide range of contaminants. However, there are also several drawbacks to using RO for nitrate removal. One major concern is the potential for brine disposal, as RO produces a concentrated waste stream that can be difficult to manage [23]. Additionally, the process can be expensive, requiring specialized equipment and maintenance.

Destructive methods convert nitrate to other nitrogen species using catalytic reduction or biological denitrification. Biological denitrification is a water treatment process that utilizes microorganisms to remove nitrate from water [24]. Microorganisms use nitrate as an electron acceptor in their respiration process, converting it into nitrogen gas that is released into the atmosphere. The microorganisms typically use a carbon source, such as methanol, as an electron donor to fuel the

process [25]. Biological denitrification can be accomplished through various systems, including packed bed reactors, fluidized bed reactors, and sequencing batch reactors. This process has several advantages, including low energy input and high treatment capacity with relatively low capital costs and environmental footprint [25]. However, the process requires careful monitoring and control to ensure that the microorganisms are functioning properly.

2.3. Catalytic nitrate removal

An attractive approach to NO_3^- treatment is the improved catalytic reduction of nitrates to nitrogen, as it does not produce secondary waste and can be tailored to the appropriate reactivity and selectivity. Nitrate could be reduced to either ammonium ($NO_3^- \rightarrow NO_2^- \rightarrow NO \rightarrow NH_2OH \rightarrow NH_4^+$) or nitrogen gas ($NO_3^- \rightarrow NO_2^- \rightarrow NO \rightarrow N_2O \rightarrow N_2$) [7]. N_2 is an environmentally friendly product, while NH_4^+ has a range of industrial applications. Both products have their merits. Under basic pH conditions, ammonium could rapidly transform to ammonia (NH_3). The production of fertilizers makes substantial use of NH_3, which is also used in the synthesis of some organic molecules, including plastics, fibers, explosives and intermediates for dyes and pharmaceuticals [26]. It is an industrially important raw material and a promising liquefied fuel [27]. Electrochemical reduction of N_2 is a way of ammonia production that has received a lot of attention recently [28]–[30]. However, N_2 is a highly thermodynamically stable compound and requires a large dissociation energy of 946 kJ/mol [31]. Studies on electrocatalytic nitrate reduction to ammonia gas are gaining substantial attention in recent years. However, due to the limitations of electrochemical processes, most of them use high initial nitrate concentrations (up to 1000 mM) to avoid the transport limitations and hydrogen evolution reaction problem of electrocatalytic performance [32]–[35]. Moreover, wastewater streams containing nitrate also include other contaminants that could interfere the process [36].

A possible alternative to physical and biological methods of removing dangerous NO_3^- from water sources is the reduction of catalytic nitrates with selectivity toward NH_4^+. Numerous materials were investigated in-depth as active catalysts and support materials for NO_3^- reduction processes, including zero-valent iron (ZVI), TiO2, hematite, NBeta, NaY zeolites, and others [37]–[41].

2.3.1. Nitrate reduction by zero-valent metals

Various chemical contaminants can be removed or degraded using ZVI, via different mechanisms, including sorption, complexation, (co)precipitation, and surface-mediated chemical

reduction [42]. ZVI is one of the most studied catalysts for nitrate reduction that has the advantages of low cost, high performance, and environmental friendliness [7]. Nitrate reduction could occur on the surface of zero-valent iron by coupled electron transfer reaction through Fe^0 oxidation to Fe^{2+} or Fe^{3+} [43]. However, particle agglomeration, formation of iron oxides on the catalyst surface, and narrow operational pH range limit the applicability of direct nitrate reduction by ZVI [42]–[44]. The use of zero-valent iron as a support material for monometallic catalysts such as Cd, Pt, Cu, and Ni was also investigated. Cu-doped ZVI was compared to meso- and nano-scaled ZVI by Liou et al. [45]. They found that the activation energies of nitrate reduction reduced more noticeably in the Cu-Fe0 system. In another study, Cu-impregnated ZVI resulted in 96% nitrate reduction in 1 h, compared to 67% achieved by Ni/ZVI under the same conditions, showing the importance of proper metal selection [46]. Cu, Ni, and other metals like Sn and Zn are referred to as promoter metals (M_p) in this context, where NO_3^- adsorption takes place with a subsequent reduction to NO_2^-. The promoter metal appears to be the primary catalyst for nitrate reduction at the ZVI-supported monometallic catalyst, with ZVI acting as a reductant source for the promoter metal, resulting in the regeneration of the oxidized promoter to the zerovalent form (for example, Cu^{2+} to Cu^0) [46]. Although numerous different catalytic systems were investigated for the removal of NO_3^- by ZVI, loss of ZVI reductive capacity and the oxidation of surface metals is the major disadvantage of prolonged nitrate removal [47].

Other zero-valent metals were also studied for nitrate reduction, including Al^0 (ZVA), Mg^0 (ZVM), Cu^0 (ZVC), and Zn^0 (ZVZ) [48]. Murphy found that ZVA has no reactivity in pH lower than 8, achieving 75% of NO_3^- removal at a pH of 10.5 with the main product being ammonia (60-95%) [49]. Similarly, Luk and Au-Yeung reported insignificant catalytic efficiency at pH lower than 10.2 and higher than 12 with a maximum removal efficiency of 62% at a pH of 10.7 [50]. Thus, nitrate removal by Al^0 is strongly reliant on pH of the reaction media. Moreover, at highly alkaline conditions, an increase in Al^{3+} ions in water was observed that possesses the necessity in additional treatment for the elimination of aluminum toxicity [48]. Different studies that used Mg^0 powder for denitrification also reported the strong influence of pH on nitrate removal efficiency. Highly acidic conditions (pH<3) resulted in the highest reactivity towards nitrate reduction [51]–[53]. Nitrogen gas was mostly found to be the product of NO_3^- reduction by ZVM.

Electrocatalysts containing cobalt are currently under great attention in denitrification applications with high ammonia selectivity [54]–[56]. According to Carvalho et al., due to the strong nitrite binding and promotion of nitric oxide dissociation, selectivity towards NH_3 is the highest for

Co among all transition metals [57]. The authors claim that the reason for this is the exceptionally high d-band center energy of cobalt metal. He et al. also suggest that Co is responsible for the conversion of NO_2^- to NH_3 in the Cu/CuOx electrocatalytic NO_3^- reduction mechanism [55]. Although cobalt is among the most used metals in electrochemical denitrification processes in recent years, its performance in aqueous catalytic systems has not been reported in the literature.

2.3.2. Nitrate reduction by bimetallic catalysts with different support materials.

To improve reactivity of monometallic catalytic systems with only M_p present, the addition of noble metal, M_n, including Pt, Pd, Ru, etc. Although M_n is not involved in the redox reaction, it is crucial in the adsorption and activation of H_2 (H_{ads}), which then decreases NO_2^- desorbed from M_p to the product, either N_2 or NH_3. In comparison to the previously described catalytic systems, bimetallic Cu-Pd/ZVI demonstrated increased reactivity, leading to a 97% reduction in 30 min under continuous H_2 flow [46].

There are other support materials used in nitrate reduction besides zero-valent iron. Passive support materials come in a variety that excel in reactivity and selectivity. These minerals include TiO_2, red mud, hematite, kaolinite, NBeta, and NaY zeolite [37]–[41]. Monometallic catalysts based on passive materials often exhibit lower or even zero reactivity when compared to Cu/ZVI due to the absence of reduction by ZVI sites [39], [58]. However, when deposited on the surface of passive support rather than on ZVI, bimetallic catalysts remove nitrate much more quickly and exhibit strong N_2 selectivity. Sn-Pd/NBeta demonstrated a 98% decrease in 30 minutes in the study by Hamid et al., with a kinetic rate constant of 19.09×10^{-2} min− and a N_2 selectivity of 80.8%, whereas Cu-Pd/NBeta demonstrated a 95% reduction in NO_3^- in 120 min, with the highest selectivity at 92% [41]. While passive support materials are not actively involved in the reaction, they contribute to varying levels of reactivity and selectivity during NO_3^- reduction. For instance, Sn-Pd/Red mud demonstrated 100% NO_3^- reduction in 45 minutes while achieving 89% N_2 selectivity [59], whereas Sn-Pd/Nbeta demonstrated 98% reduction in 30 minutes while producing a lesser N_2 selectivity of 80% [41]. The mechanical characteristics of the support material and its interactions with the metal play a significant part in how well the catalyst functions [7]. Deactivation by surface fouling, irreversible oxidation of the promoter metal, metal leaching, and metal particle aggregation are some of the major difficulties that catalytic NO_3^- removal systems encounter.

2.4. Metal-organic and zeolitic-imidazolate frameworks

A relatively recent family of extremely adaptable materials known as metal-organic frameworks (MOFs) is composed of metal ions coordinated to organic linkers that create highly organized three-dimensional structures [60]. Numerous metal-ligand (one or more) couples can create MOFs with any required mechanical properties. MOFs found applicability in many research areas, including gas separation, drug delivery, energy storage, photo- and electrocatalysis [61]–[63]. Among the appealing qualities of MOF materials for catalytic applications are their large surface area, variable pore size, and shape. Due to the aforementioned properties, the ability to add guests, a variety of post-synthesis changes, and simple synthetic processes, the application of MOFs as heterogeneous catalysts is developing quickly [60]. As heterogeneous catalysts, MOFs have been successfully tested for oxidations of olefins, reduction of nitroaromatics, oxidation of alcohols, etc. [64].

Zeolitic-imidazolate framework materials (ZIFs) are a sub-class of MOFs, which gained great attention due to their tunable characteristics, environmentally friendly and facile synthesis techniques, and competitive stability [65]–[68]. ZIFs made up of M-im-M molecules where M stands for Zn, Co cation and im stands for the imidazolate linker that self-assembles during the synthesis process. ZIFs have a variety of topologies that resemble traditional aluminosilicate zeolites, where metal ions act as silicon and imidazolate anions act as oxygen by forming bridges [69]. ZIFs thus frequently take on zeolite-like topologies with structures resembling those found in zeolites.

Nevertheless, there is a lack of research efforts being devoted to the application of MOFs and ZIFs for the catalytic removal of NO_3^- [70]. Papers published recently consider mainly the application of MOFs for electrochemical nitrate reduction to N_2 or NH_4^+, and photocatalytic reduction to ammonium [71]–[73]. In fact, very few studies used metal-organic framework catalysts for this purpose so far. MOFs and ZIFs have not found their application in aqueous catalytic nitrate reduction yet. The selection of appropriate MOFs could be challenging due to some disadvantages of these materials. One of the strongest criticisms of the application of MOFs in heterogeneous systems is the lack of structural stability in certain solvents. For example, ZIF-8 and ZIF-67 are known to be unstable under acidic conditions [74], [75]. The low acidic stability of ZIFs is caused by the fairly strong affinity between protons and azolate groups [76]. The structures of ZIFs are present in Figure A1. Overall, the main disadvantage of MOFs is their water instability due to the lability of ligand–metal bonds [77]. ZIFs with open metal sites strongly bind water and are difficult to regenerate after water exposure. Various post-synthetic treatment ways are available to modify ZIFs according to the desired

properties. Carbonization of ZIFs results in highly stable carbon materials that are also under substantial investigation due to their high surface area, controllable pore size, and improved stability compared to their precursors [8], [78], [79].

Chapter 3 – Methodology

3.1. Materials

Sodium nitrate (99.0%, ACS reagent, Sigma Aldrich) and sodium nitrite (99.0%, Sigma Aldrich) were used to prepare calibration standards for ion chromatography and for batch kinetic experiments. Cobalt(II) nitrate hexahydrate (≥98.0 %, Sigma Aldrich), and 2-Methylimidazole (99.0%, Sigma Aldrich) were used for the synthesis of ZIF-67. Eluents for ion chromatography were prepared with 100 mM H_2SO_4 solution (96%, ACS reagent, Sigma Aldrich) for suppressor regeneration, and 1.0 mM $NaHCO_3$ (99%, ACS reagent, Sigma Aldrich), and 3.2 mM $NaCO_3$ (99.8%, ACS reagent, Sigma Aldrich) as buffer. All solutions were prepared with deionized water (18 MΩ*cm). The precursor solutions for promoter metals were prepared with Tin (IV) chloride pentahydrate (99.0%, ACS reagent), Copper (II) chloride dehydrate (98.0% Sigma-Aldrich), Ruthenium(iii) chloride hydrate (99.98% trace metal basis, Sigma-Aldrich), Nickel (II) chloride (98%, Sigma-Aldrich). Disodium tetrachloropalladate (98% Sigma-Aldrich), Platinum(IV) chloride (99%, ACROS Organics, USA) were also used as Pd, Pt precursors for noble metals, respectively. $NaBH_4$ (99%, Sigma Aldrich) was used for catalyst reduction. 99.8% CO_2 was used for buffering of the reaction media and 99.9% N_2 was used to deaerate DI water to operate in anaerobic conditions.

3.2. Synthesis of ZIF-67

ZIF-67 was synthesized by mixing 0.291 g of $Co(NO_3)_2*6H_2O$ (1 mmol) with 0.66 g of 2-methylimidazole (8 mmol) in methanol at room temperature [80]. The solution was stirred vigorously for 24 h. The precipitated product was separated by centrifugation at 8000 rpm for 6 min and washed with methanol three times. The solid product was dried to remove the solvent at room temperature under a vacuum overnight.

3.3. Synthesis of Co@NC

ZIF-derived Co@N-doped carbon composite material, Co@NC, was obtained by direct carbonization of ZIF-67 in a tube furnace at constant Ar flow. The following heating procedure was applied: first, heating to 100°C with a ramping rate of 4°C/min and maintenance time of 2 h for the removal of moisture absorbed on the surface of ZIF and ensuring fully anaerobic conditions, then heating to 900°C with a rate of 3°C/min for 4.4 h and maintaining this temperature for 3 h. After the tube furnace naturally cooled down, the obtained black powder (Co@NC) was dispersed in 0.1M HCl

at room temperature overnight to remove loosely attached Co nanoparticles on the surface. Finally, the material was washed two times by water and dried at 80°C.

3.4. Synthesis of bimetallic catalysts

Metallic catalysts were synthesized on the surface of Co@NC by the incipient-wetness co-impregnation method [81]. First, 0.5 g of support material was added to 25 ml of DDIW and ultrasonicated for 6 min for uniform dispersion in suspension. Then, the required amount of metal salts was weighed by calculating the percentage (0.5 - 3.6%) out of support mass and dissolved in 15 mL of water. Then, metal precursor solution was added dropwise to the Co@NC suspension under constant stirring. The solution was stirred for 2 hours to ensure all metal particles were attached to the surface. Afterward, the materials were washed two times with DI water and dried to remove moisture at 80°C overnight.

The flow diagram of catalyst synthesis is illustrated in Figure 1.
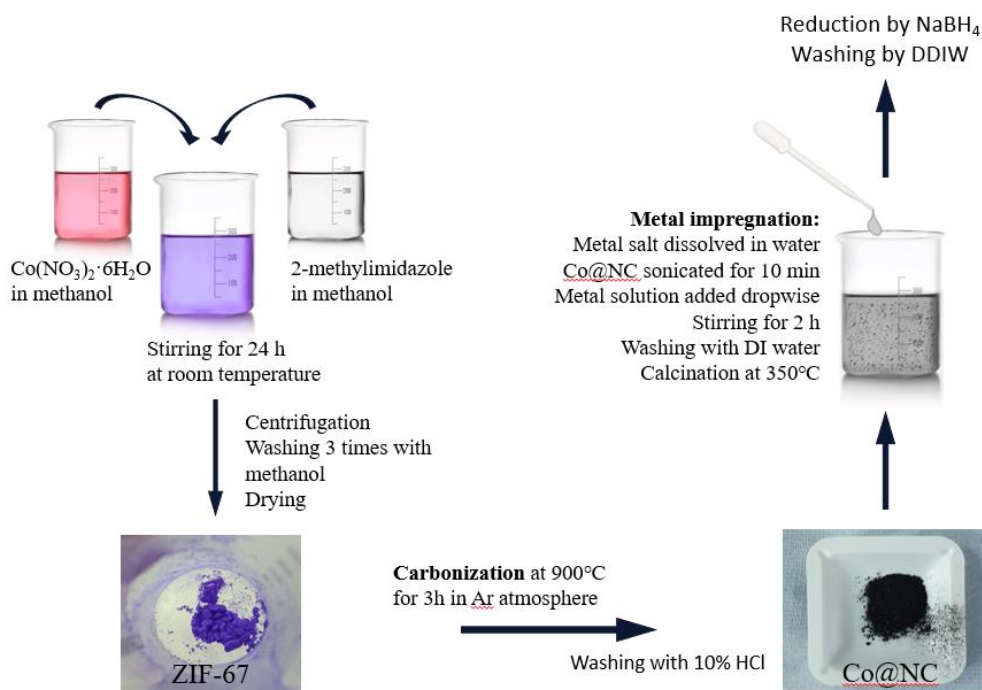
Figure 1. Catalyst synthesis procedure

3.5. Catalyst characterization procedure

Materials morphology and particle shape were identified by SEM (Zeiss Crossbeam 540, Germany). Before the analysis, all samples were coated by 5 nm Au layer for improved conductivity.

TEM (JEM 1400Plus, JEOL, Japan) at the accelerating voltage of 120 kV was used with samples dispersed beforehand in ethanol by ultrasonication and placed on carbon-coated copper grid followed by drying overnight. SEM/EDS (JSM-IT200, JEOL, Japan) was used to identify elemental distribution on the surface of prepared materials. XRD patterns were obtained by D2 SmartLab (Rigaku) equipment with graphite monochromatized Cu Kα radiation (λ=1.540598Å). The analysis mode was 40kV & 50mA, where a scan rate was 0.05^o/s in a 2θ range of 5-70°. The Simultaneous Thermal Analyzer (STA) 6000 (PerkinElmer) was used to analyse the thermal stability of materials from room temperature to 800 °C in the inert atmosphere under the heating rate of 5 °C min^{-1}. FTIR spectrometer (NICOLET iS10, Thermo) with a Smart OMINI-Transmission Accessory was used for the analysis of functional groups present on the materials surfaces. The IR spectra (4000–400 cm$^-$) were recorded at a resolution of 4 cm$^-$ by averaging 50 scans. The mixture of powders (mass ratio of KBr to sample was 1000:1) was transferred to a 7-mm pellet die, and the KBr pellet was analyzed after fabrication with a pellet press. Zetasizer Nano ZS (Malvern Panalytical, UK) was used to identify the zeta potential of materials after 24 h stirring in aqueous dispersant at initial pH values of 3.0; 5.0; 7.0; 9.0; 11.0, and 13.0 that cover acidic, neutral, and basic conditions. To investigate the changes on catalyst surface after reaction, X-ray photoelectron spectroscopy (XPS) was performed before and after the reaction by NEXSA (Thermo Scientific) using a monochromated low-power Al Ka X-ray source of 1486.6 eV. Samples were dried if needed and stored in anaerobic conditions prior to analysis. Metal leaching from the catalyst surface was identified by ICP-OES iCAP 6300 (Thermo Fisher Scientific, USA) for Cobalt and ICP-MS iCAP RQ (Thermo Fisher Scientific, USA) for Pt.

3.6. Nitrate reduction kinetic experiments

Catalytic nitrate reduction was studied at room temperature and pressure in an anaerobic environment. The reaction environment was preliminarily prepared by purging 100 ml of DI water in a three-necked reactor with H_2 to remove dissolved oxygen and saturate with hydrogen gas. Before the reaction started, the 0.25 g of catalyst was reduced by 0.1 M $NaBH_4$ in deaerated deionized water. pH was stabilized by CO_2 that was continuously supplied to the reactor. The reaction was initiated by adding nitrate salt stock solution to the reactor containing a reduced catalyst. The initial nitrate concentration was 60 mg/L NO_3^-- N, corresponding to 272.7 mg/L of NO_3^-. All kinetic experiments were performed for 60 minutes and in duplicates with standard deviation as indication of error.

Samples were collected and filtered using a 0.2 µm membrane syringe filter. The concentrations of NO_3^-, NO_2^- and NH_4^+ were measured at each sampling time. The filtered samples

were analyzed for NO_3^- and NO_2^- by ion chromatography 930 Compact IC Flex (Metrohm, Switzerland) with an anionic column (Metrosep A Supp 5 - 250/4.0). Ammonium product was identified by cationic column (Metrosep C 4 - 150/4.0).

An ion chromatography method was prepared using 0, 0.5, 1, 5, 10, 15, 20, and 30 mg/L standards for NO_3^-, NO_2^-, NH_4^+. Na^+ was added to the ion chromatography method to distinguish ammonium from sodium peaks that appear close to each other on the chromatogram. Calibration curves used in all IC measurements are presented in Figures A1-A4. Nitrogen gas was calculated according to the mass balance, assuming that intermediate products were fully converted during the reaction. After the reaction, the catalyst was collected for surface characterization for characterization by XPS.

Kinetic rate constants for nitrate removal were calculated using pseudo-first-order kinetics:

$$\ln\left(\frac{C}{C_0}\right) = k_1 t \tag{1}$$

where C_0 represents the initial concentration of $NO_3{-}N$, while C is the concentration at time t. First order kinetic rate constant is represented as k_1 with the unit of min^{-1}.

Additionally, desorption experiments were designed in the following way to remove nitrogen species from the surface of the catalyst. After 60 min of nitrate reduction reaction, the catalyst was collected by centrifugation and washed 2 times with DI water. Then, the catalyst was treated with 0.01 M HCl solution by vigorous stirring for 12 h.

The NO_3^- removal and byproduct selectivity was calculated by the following equations [82]:

$$R_{NO_3^-}(\%) = \frac{[NO_3^- - N]_i - [NO_3^- - N]_f}{[NO_3^- - N]_i} \times 100 \tag{2}$$

$$S_{NO_2^-}(\%) = \frac{[NO_2^- - N]_f}{[NO_3^- - N]_i - [NO_3^- - N]_f} \times 100 \tag{3}$$

$$S_{NH_4^+}(\%) = \frac{[NH_4^+ - N]_f}{[NO_3^- - N]_i - [NO_3^- - N]_f} \times 100 \tag{4}$$

$$S_{N_2}(\%) = \frac{[NO_3^- - N]_i - [NO_3^- - N]_f - [NO_2^- - N]_f - [NH_4^+ - N]_f}{[NO_3^- - N]_i - [NO_3^- - N]_f} \times 100 \tag{5}$$

The subscripts i and f represent the concentrations at the initial and final conditions, respectively, for each ion.

The effect of operating parameters was evaluated by fixing reaction conditions at a catalyst loading of 2.5 g/l, metal loading of 3.6%, contaminant concentration of 60 mg/l of NO_3^-N, H_2 flow, pH of ~5.8 maintained by CO_2 flow, except for the varied condition. A durability and stability study was done in repeated reaction cycles where the catalyst was washed by DDIW after each reaction cycle and returned to the reactor without regeneration. While the catalyst was centrifuged and washed, fresh reactor media was prepared by N_2 flow as before the first reaction. Cobalt and Platinum leaching from the catalyst's surface was measured in each collected sample.

Chapter 4 – Results and Discussion

4.1. Materials characterization

Scanning electron microscopy (SEM) and transmission electron microscopy (TEM) were used to examine the morphology and microstructure of the materials. Figure 2 shows SEM images at 20K and 50K magnifications to visualize morphological differences between ZIF-67, Co@NC, and Pt-Co@NC. Figure 2(a-b) shows that ZIF-67 crystals have a cubic morphology with well-defined faces and sharp edges. The crystals are uniform, with the average size of about 240 nm. These results are consistent with previous reports, indicating successful synthesis of ZIF-67 [80], [83]. The carbonization process transforms the original zeolitic framework of the ZIF-67 into a more irregular carbon-based material, Co@NC, while maintaining its porous structure (Figure 2(d-e)). The particle size of Co@NC was decreased to 190 nm due to the decomposition and shrinkage during the annealing process, and its surface became rough. The morphology and size of ZIF-67 change when it is carbonized because the carbonization process involves the removal of the organic ligands that hold the metal ions together in the original ZIF-67 structure. These ligands are typically thermally unstable; at elevated temperatures, they decompose, resulting in structural collapse. The carbonized nanoparticles are densely packed, forming a mesoporous structure with a large surface area. Impregnation of Co@NC surface by Pt did not affect the material's morphology. EDS elemental mapping in Figure 2(c) shows low Co weigh percentage on the material's surface (27.85±1.29) in comparison to Figure 2(f), where more Co is exposed to the surface (52.4±1.33). Almost double increase in Co content on the surface is explained by the breakage of metal-organic links holding Co inside the ZIF-67 structure. Due to the thermal treatment, nitrogen content was not significant in carbonized materials. Elemental mapping is resented in Figure A5. Pt was uniformly distributed on the Co@NC surface after impregnation and calcination, as seen from Figure A5(c), indicating successful catalyst synthesis.
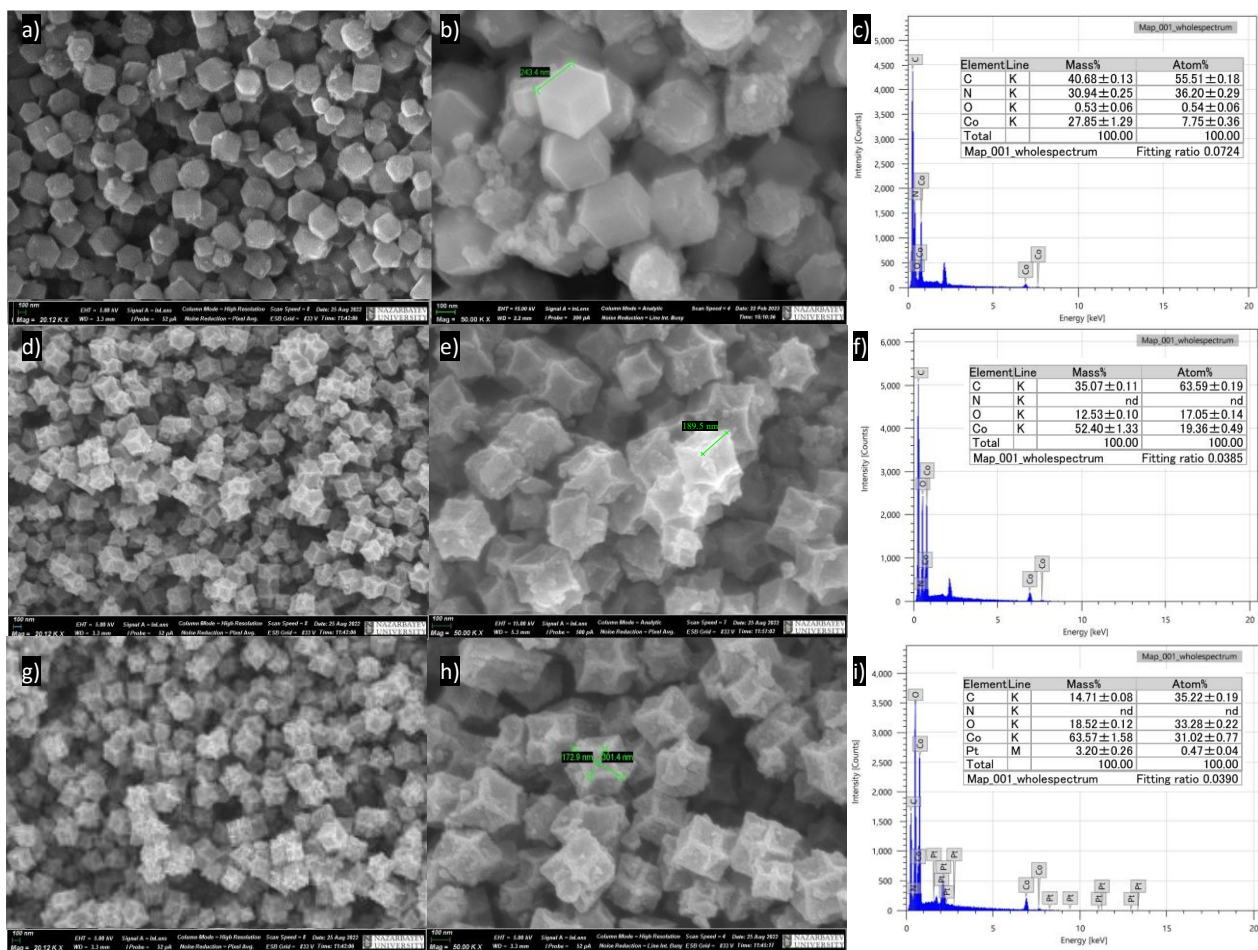
Figure 2. SEM images of ZIF-67 (a-b), Co@NC (d-e), Pt-Co@NC (g-h); EDS elemental spectrum with quantitative distribution of ZIF-67 © Co@NC (f), and Pt-Co@NC (i).

A TEM image of a ZIF-67 particle in Figure 3(a) shows a well-defined crystalline structure with a characteristic polyhedral shape. A carbonized material, Co@NC has a dark, amorphous region surrounded by a brighter halo in Figure 3(b). The dark region corresponds to the carbonized portion of the particle, while the brighter halo is attributed to the amorphous carbon coating that forms around the particle during carbonization. The shape of the carbonized particle remained similar to ZIF-67, although less defined. Pt-Co@NC has a smaller particle size and smoother edges due to calcination (Figure 3(c)).
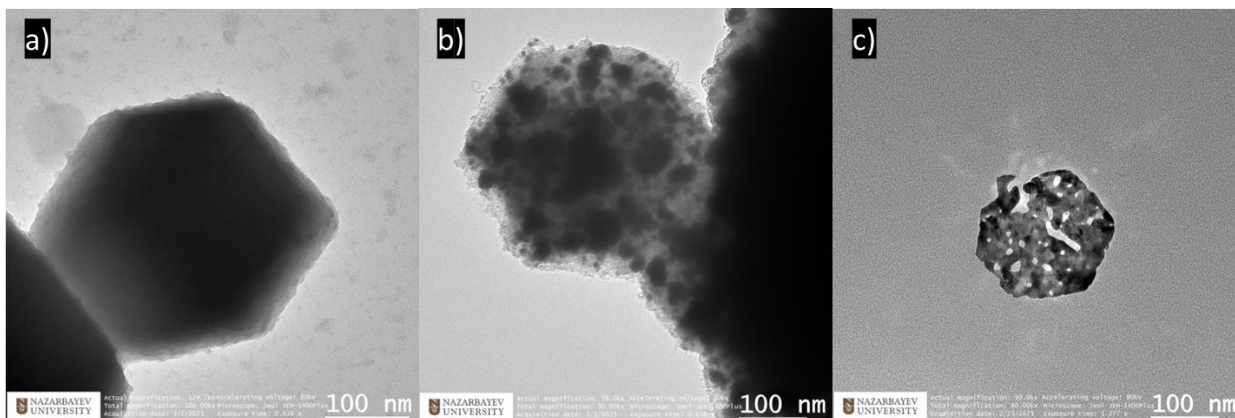
Figure 3. TEM images of ZIF-67 (a), Co@NC (b), Pt-Co@NC (c).

TGA analysis was performed to understand the thermal behaviour of ZIF-67 under carbonization. The TGA curve in Figure 4 shows a weight loss attributed to the structure's thermal decomposition of the organic ligands. This weight loss is observed as a steep drop in the TGA curve, occurring at a temperature of around 500 ℃. As the temperature increases, the slower weight loss continues without reaching a plateau, indicating the incomplete removal of the organic ligands. The TGA curve of Co@NC shows a weight loss due to removing residual organics and other impurities. This weight loss is observed as a gradual decrease starting at temperatures of 500 ℃.
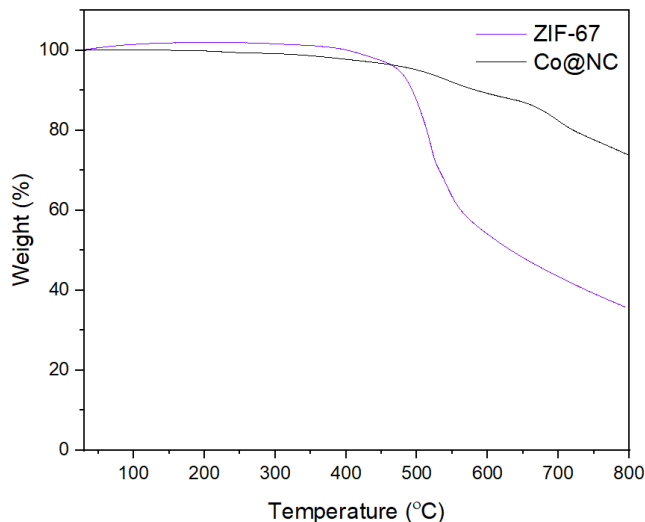
Figure 4. TGA analysis of ZIF-67 and Co@NC.

Fourier transform infrared spectroscopy was used to identify synthesized materials' chemical compositions and structural characteristics. In Figure 5(a), ZIF-67 absorption bands confirm the successful synthesis of ZIF-67 and the presence of the expected chemical functional groups in the material [84], [85]. FTIR spectrum shows a signal at 425 cm^{-1} related to the Co–N stretching vibration due to the coordination between Co and the N atom of the organic linker. Absorption bands

at 693 cm^{-1} and 757 cm^{-1} correspond to the out-of-plane bending of the imidazole ring [85]. Two peaks at 992 and 1141 cm^{-1} are attributed to bending and stretching vibrations of the C-N bond in the aromatic ring. Aliphatic and aromatic C-H stretch of 1,3- diazole are seen from two bands detected at 2962 and 3136 cm^{-1}, respectively [86]. The broad peak located at 3250-3600 cm^{-1} is ascribed to the vibration of O–H in the bonded water. The FTIR spectrum of Co@NC shows a significant reduction in the intensity and disappearance of some ZIF-67 characteristic bands. As mentioned previously, this is due to removing the organic ligands that held the metal ions together in the original ZIF-67 structure.

The crystal structure of ZIF-67, Co@NC and Pt-Co@NC was studied by XRD analysis. XRD can provide information on the crystal structure of the original ZIF-67 material and the changes that occur during the carbonization and Pt doping process. In Figure 5(b), the ZIF-67 diffractogram shows sharp peaks indicating the material's high crystallinity. All major peaks of ZIF-67 were indexed corresponding to the unit cell dimensions of the material. ZIF-67 XRD results are in excellent agreement with the literature [87]–[89]. During the carbonization process, the organic ligands in ZIF-67 are decomposed, and the resulting material loses the crystallinity of ZIF-67 precursor. As a result, the XRD pattern of Co@NC does not show peaks corresponding to the ZIF-67 structure. This is due to the loss of the ordered crystal structure of ZIF-67 during the carbonization process that was seen on FTIR as well. The XRD pattern of Co@NC shows new peaks corresponding to cobalt metal. During pyrolysis, cobalt becomes incorporated into the carbon-based material, resulting in the appearance of cobalt peaks in the XRD pattern of carbonized ZIF-67. After Pt doping on the surface of Co@NC, XRD reveals additional peaks that were matched to the Pt.
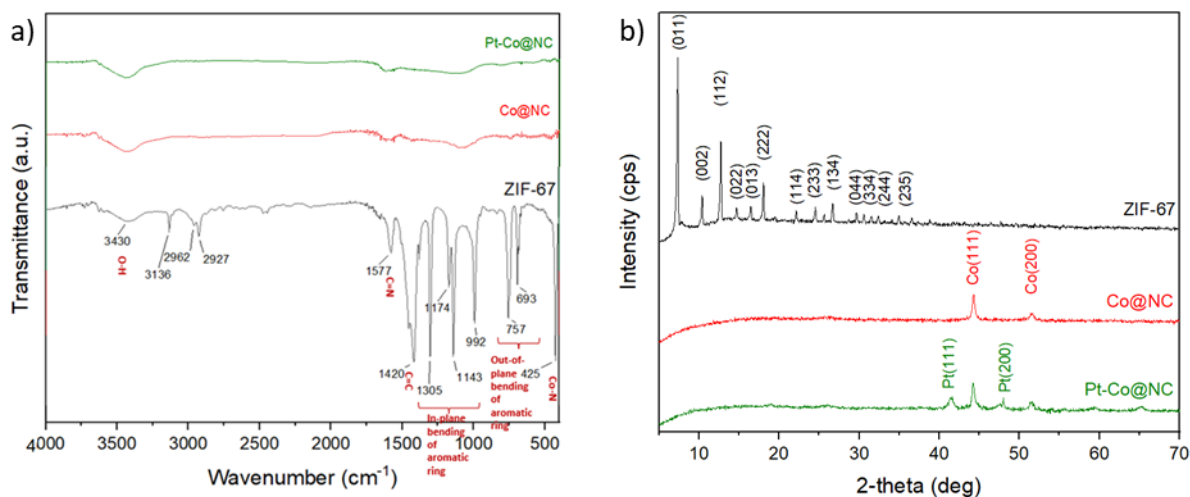
Figure 5. FTIR (a) and XRD (b) of ZIF-67, Co@NC and Pt-Co@NC.

Another important property of heterogeneous catalysts is their surface charge under various conditions. The change of zeta potential values over a wide pH range for Co@NC and Pt-Co@NC is shown in Figure 6. The results illustrate that the zeta potential of Co@NC decreases rapidly when the solution pH increased to 5 with some minor fluctuations up to pH 5-9, after which the surface is negatively charged. The point of zero charge for Co@NC was found to be pH_{pzc} of 9.41. Impregnation of Co@NC surface by Pt shifted pH_{pzc} to more neutral value of 7.14. The increased acidic properties of the catalyst surface reveal that the degree of protonation is significantly affected by Pt impregnation. At a pH lower than pzc, the material charges positively and adsorbs preferentially anions (NO_3^- and NO_2^-), while at higher pH values, the surface would attract positively charged ions (NH_4^+). To enhance NO_3^--N removal, it is desired to keep reaction media at pH values lower than pH_{pzc} to promote the sorption of nitrate anions on the catalyst surface for further reduction.
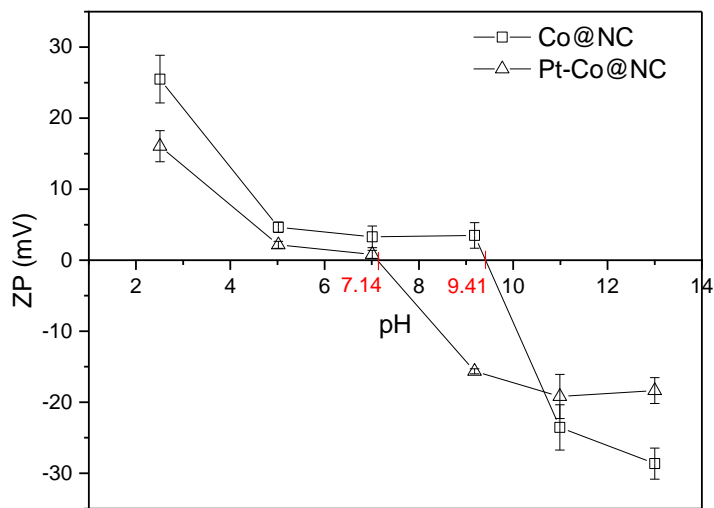
Figure 6. Zeta potential of Co@NC and Pt-Co@NC.

4.2. Catalytic nitrate reduction by Pt-Co@NC

Figure 7 shows the NO_3^-–N removal kinetics by different materials, including homogeneous reaction with $NaBH_4$ and reduction by ZIF-67, Co@NC and Pt-Co@NC in the presence of H_2 flow. The initial contaminant concentration is 60 mg/l of NO_3^-–N, corresponding to 265.6 mg/l of NO_3^-, and the reducing agents loading is 2.5 g/L. Homogeneous reduction by 0.1 M $NaBH_4$ or under H_2 flow without the addition of catalyst was insignificant, as well as with the addition of ZIF-67. Co@NC showed 7.23% of NO_3^--N removal indicating that without metal impregnation, the system is not reactive enough. Non-reduced Pt-Co@NC did not show any sorption of nitrate. Pt-Co@NC demonstrates complete nitrate reduction under H_2 flow in 30 min with pseudo-first-order kinetic rate

constant of 0.114 min^{-1} (R^2=0.936) with 100% conversion to NH$_4^+$-N. The mass balance showed 97.18% of total nitrogen in bulk solution by the end of the reaction. After desorption for 24h with 0.1 M HCl, an additional 1.12% of total N was recovered in the form of NH$_4^+$-N and 0.5% as NO$_3^-$N, summing up to 98.8% of nitrogen and 99.5% of NH$_4^+$-N selectivity. The complete nitrate reduction profile with concentrations of NO$_3^-$-N, NO$_2^-$-N, and NH$_4^+$-N is shown in Figure 7(b).
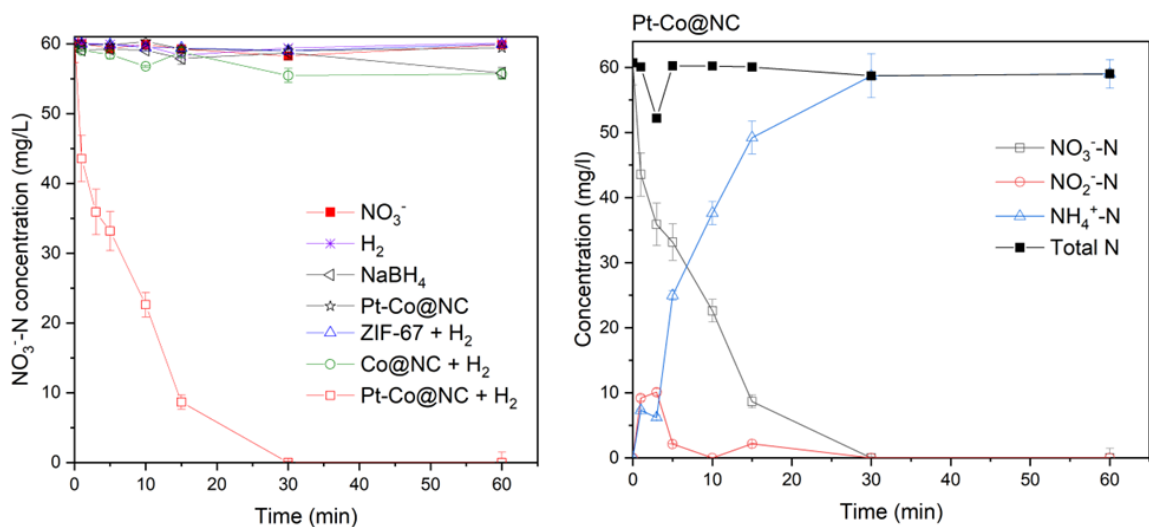
Figure 7. NO3--N removal in control tests, Co@NC, ZIF-67, Pt-Co@NC (a); and NO3--N reduction to NO2--N and NH4+-N by Pt-Co@NC (b).

Although most of the nitrate reduction studies are focused on N$_2$ selectivity, and NH$_4^+$/ NH$_3$ selectivity is mostly achieved by electrochemical processes, Table 1 summarizes some of the previously reported results with high reactivity or NH$_4^+$ selectivity to compare the results obtained in this study. 3.6%Pt-Co@NC is able to provide one of the fastest reactivities for nitrate removal with high NH$_4^+$ selectivity in both low and high contaminant loadings.

Table 1. Reactivity and selectivity in different catalytic systems

| Catalyst	NO_3^- concentration (mg/l)	NO_3^- removal (Time)	k_1 (x 10^{-2} min^{-1})	NH_4^+ selectivity (%)	Other experimental conditions	Ref.
3.6%Pt-Co@NC	265	1.00 (30 min)	11.4	99.5		This work
3.6%Pt-Co@NC	265	1.00 (30 min)	14.6	76.6	Initial pH 3.0	This work
3.6%Pt-Co@NC	22	1.00 (5 min)	50.9	98.2		This work
1.0%[$Cu_{0.63}$-Pd]@AC	200	0.686	0.356	27.0	Continuous up-cocurrent flow reactor	[90]
2.2%Sn-1.6%Pd@N-Beta	133	0.98 (30 min)	19.09	0.192	H_2, CO_2 flow Catalyst dose: 2.5 g/L	[91]
1%Pd-0.3%Cu@AC	100	0.44 (5 h)	-	74.0		
1%Pt-0.1%Cu@AC	100	0.27 (5 h)	-	0.79	H_2+CO_2 (1:1) gas flow (rate 200 $Ncm^3 min^{-1}$)	[92]
1%Rh-0.3%Cu@AC	100	0.9 (5 h)	-	0.97		
1%Ir-1%Cu@AC	100	0.35 (5 h)	-	0.89		
1%Pd-1%Cu@TiO_2	100	1.00 (5 h)		0.83		
1%Pd-1%Cu@CNT-TiO_2	100	1.00 (5 h)		0.34		[93]
0.2%Pd-4%Cu@Al	142	1.00 (4 h)	1.87	0.885	pH 4.0, no gas flow	
4%Cu@Al	142	1.00 (4 h)	2.88	99.9	Catalyst dose: 3.53 mmol/L	[94]

4.3. Evaluation of factors affecting nitrate reduction kinetics

4.3.1. Effect of metals on the surface of Co@NC

The selection of Pt-Co@NC was done based on the evaluation of different metals impregnated on the Co@NC surface. Figure 8 shows the reduction profiles by 3.6%wt metals, including Cu, Pt, Pd, Sn, Ru, Ni. Among all metals, Pt showed a complete reduction of NO_3^-N, as discussed previously. Cu-Co@NC, Ni-Co@NC and Sn-Co@NC removed only 51.7%, 70.5% and 32.7% in 60 min, respectively. Ru-Co@NC showed a sorption-like profile, removing 32.7% of NO_3^-N in the first minute without further changes in the nitrate concentration and showing 4.4% selectivity to NH_4^+. Only 17.7% of total N was detected in bulk solution, while the mass balance was kept in all other reactions. Loss of N species in bulk could be due to conversion to N_2 or sorption of products or reactants on the catalyst surface. The reactivity of metallic catalysts strongly depends on the type of

metal, while selectivity to NH_4^+-N was high for all cases except for Ru-Co@NC. Table 2 summarizes the kinetic results for different metallic catalysts.
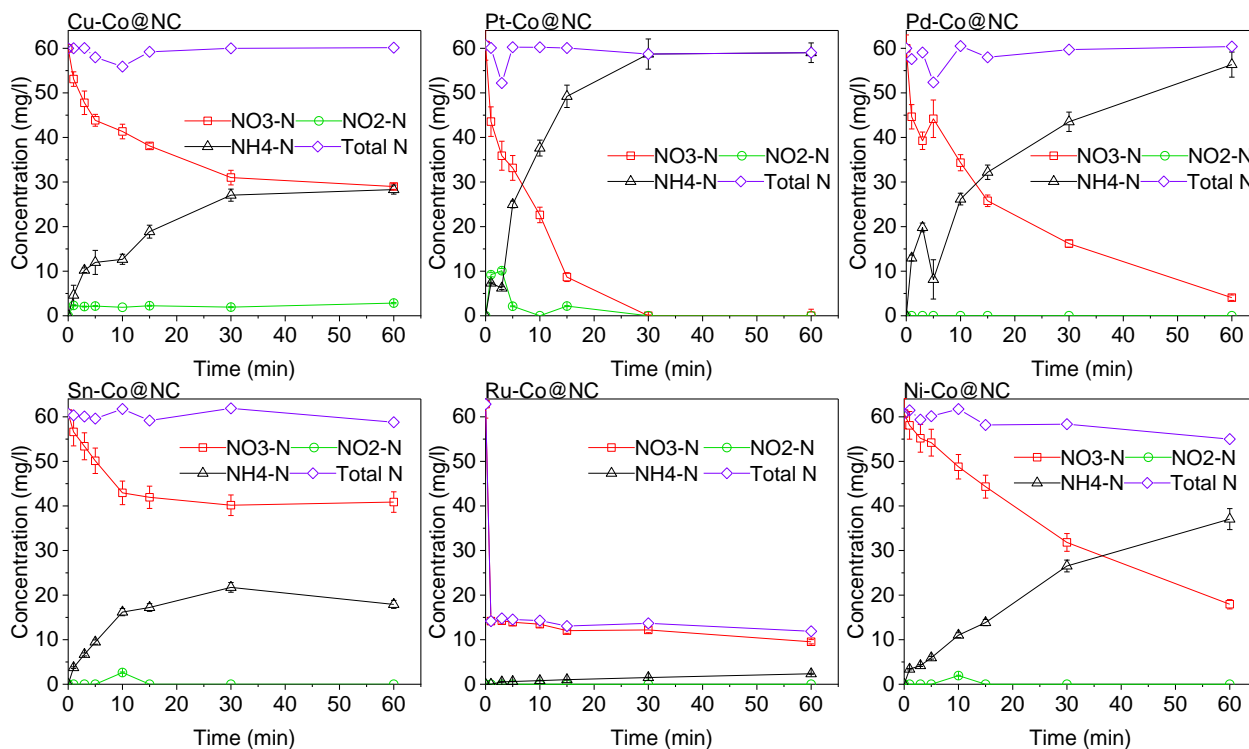
Figure 8. Nitrate reduction profiles for different metals doped on the surface of Co@NC.

Table 2. Summary of kinetic results of nitrate reduction by different metals doped on the Co@NC surface.

	Cu	Pt	Pd	Sn	Ru	Ni
$R_{NO_3^--N}(\%)$	51.7%	100.0%	91.6%	32.7%	84.3%	70.5%
$S_{NH_4^+-N}(\%)$	91.3%	99.5%	98.9%	90.2%	4.4%	86.6%
$k_1(min^-)$	0.011	0.114	0.038	0.006	0.014	0.020
R^2	0.743	0.937	0.982	0.449	0.136	0.999

4.3.2. Effect of Pt loading on the Co@NC surface

The loading of the metals can play a significant effect on catalytic performance affecting both the selectivity and reactivity of the catalyst [7]. Different studies show that an increase in noble and promoter metal loading demonstrates a volcano-shaped NO_3^- reduction dependence [95]–[97]. An increase of Pt loading from 0.5% to 3.6% resulted in an increase in rate constant from 0.012 to 0.114 min^{-1} in Figure 9.
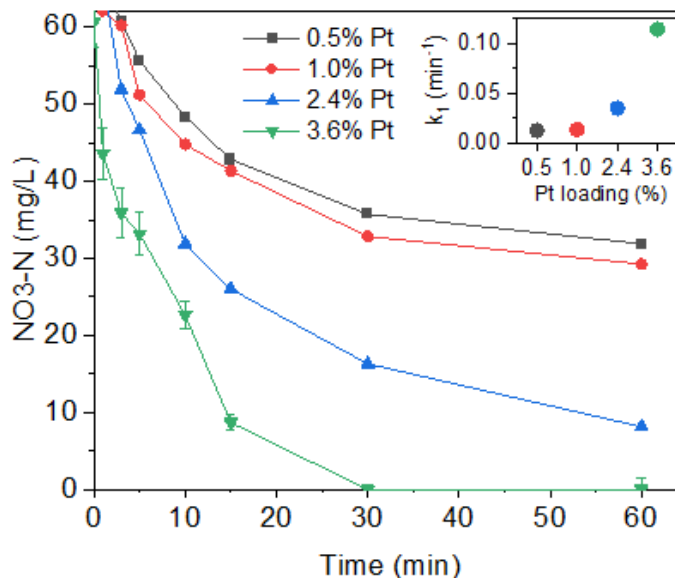
Figure 9. Effect of Pt loading on the NO_3^-- N removal.

4.3.3. Effect of initial contaminant concentration

Higher concentrations of NO_3^- typically result in a lower removal rate due to less available active sites on catalyst surface. Lower nitrate concentrations, thus, result in faster removal rates. Pt-Co@NC showed 54.3% reduction of 100 mg/l, but concentrations up to 60 mg/l were removed completely. An initial concentration of 5 mg/l was reduced in 5 minutes, while 15 mg/l removal was achieved in 15 min.
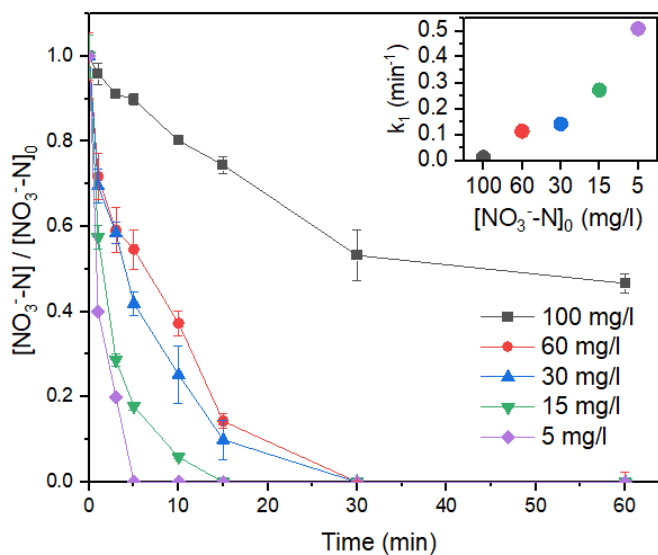
Figure 10. Effect of initial contaminant concentration on NO_3^-- N removal rate.

4.3.4. Effect of catalyst loading

Higher catalyst loading offers more active sites for nitrate reduction leading to an enhanced NO_3^-–N removal rate [98]–[100]. In Figure 11, catalyst loading of 2.0 g/l resulted in 77% removal of NO_3^--N, while 2.5 g/l provides full reduction of nitrate in 30 min. Further increase in catalyst loading resulted in higher kinetic rate constant of 0.241 min^{-1}. NH_4^+-N selectivity was independent of catalyst loading and maintained at 97.2-99.5% in all reactions showing a slight trend towards higher selectivity at higher catalyst loading. Catalyst loading significantly affected reactivity of the process without difference in product selectivity.
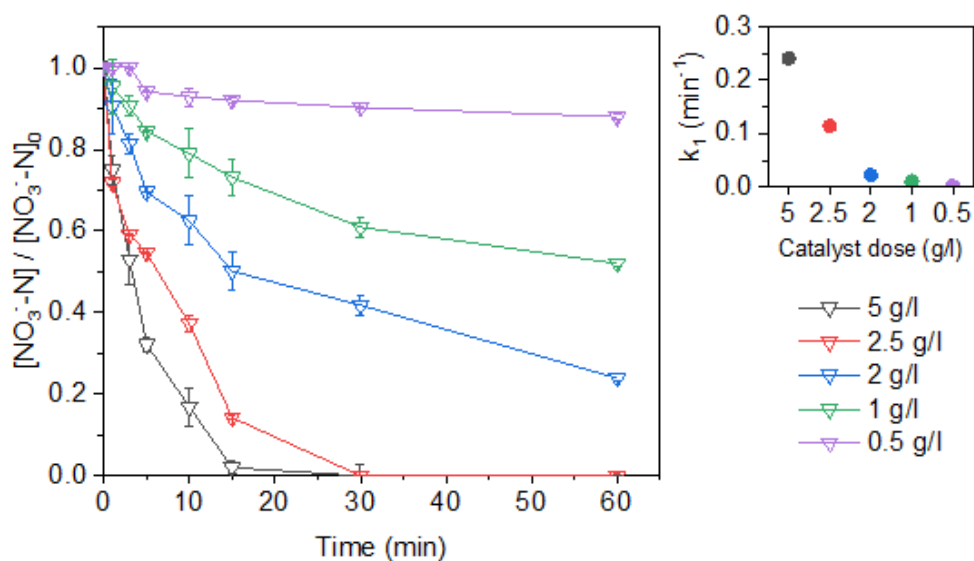
Figure 11. Effect of catalyst loading on NO_3^-- N removal rate.

4.3.5. Effect of pH

Kinetic experiments described in previous sections were performed under CO_2 flow to maintain pH at ~5.6. However, the media's pH significantly affects the reactivity and selectivity of the catalytic system. In Figure 12, the initial pH of the system was varied between 3-11 by adding HCl and NaOH solutions. At initial pH values up to 7, full NO_3^-–N removal was 100%, while at pH of 11, reactivity of 96.3% was observed. pH_{pzc} of Pt-Co@NC, which was found to be at 7.14 is well agreement with these results, showing that affinity of NO_3^- is one of the factors affecting the performance of catalytic system. From Table 3, the fastest nitrate reduction rate of 0.137 min^{-1} was observed at initial pH of 3, then pH 5 and 7 showed similar k_1 value of 0.082 min^{-1} and, finally, at pH 11 the rate was 0.053 min^{-1}. In contrast to the reactions performed under constant CO_2 flow, where mass balance was typically maintained at values higher than ~97%, total nitrogen was decreased in all reactions where only initial pH was adjusted.
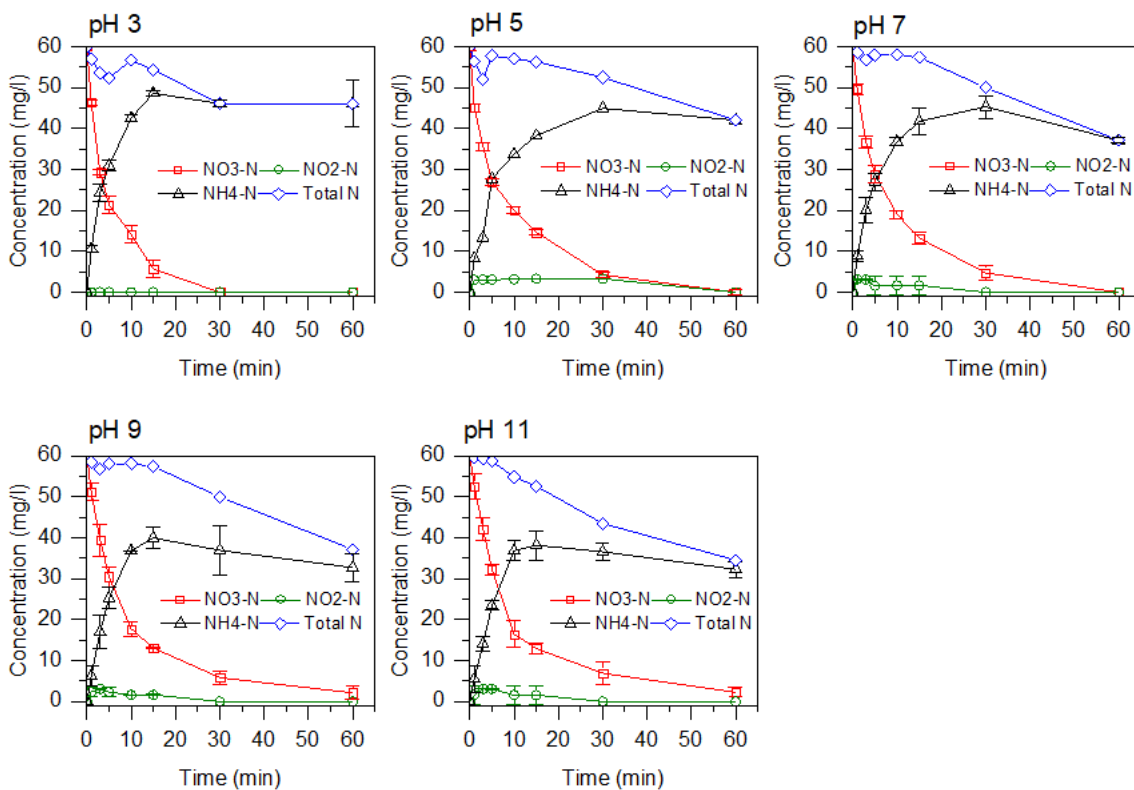
Figure 12. The effect of initial pH on NO_3^-N removal rate.

Table 3. Summary of kinetic results of nitrate reduction by different initial pH values.

pH	3	5	7	9	11
$R_{NO_3^--N}(\%)$	100.0	100.0	100.0	98.13	96.28
$S_{NH_4^+-N}(\%)$	76.6	70.0	61.8	55.2	55.8
$k_1(min^-)$	0.146	0.082	0.082	0.054	0.053
R^2	0.964	0.978	0.978	0.922	0.928

4.3. The surface analysis of Pt-Co@NC after nitrate reduction.

To investigate the catalyst surface after reaction, XPS analysis was performed before and after reaction as shown in Figure 13. All the peaks were shifted in order to adjust C1s peak to 284.8 eV. Figure 13(a) shows two characteristic peaks at 783.4 and 798.1 eV with no shake-up satellites corresponding to the most primary cobalt species Co_3O_4 in unreduced catalyst. After reduction by $NaBH_4$, $Co2p_{1/2}$ and $Co2p_{3/2}$ peaks were observed at 798.96 and 783.0 eV with satellite features at 804.52 and 786.8 eV, respectively. This corresponds to the Co^2. Moreover, there is an overlap with Co LMM Auger peak at 775 eV indicating the presence of Co^0. After 1 h of NO_3^- reduction, mixed oxidation state of Co^{2+} and Co^{3+} is observed. Pt4f region has well separated spin-orbit components. Difference between two peaks for metallic Pt form is 3.35eV, which is seen in Figure 13(h). Peaks in

the Pt4f region have an asymmetric peak shape for platinum metal. This indicates that after reaction with NO3-N, Pt keeps metallic Pt^0 form. While Co oxidation states partially undergone changes during reaction from Co^{2+} to Co^{3+}, Pt oxidation state does not change, which agrees with mechanisms reported in literature, where noble metal does not participate in the redox reaction and remains in the metallic form [7]. Further study is required to suggest the mechanism of catalytic nitrate reduction by Pt-Co@NC.
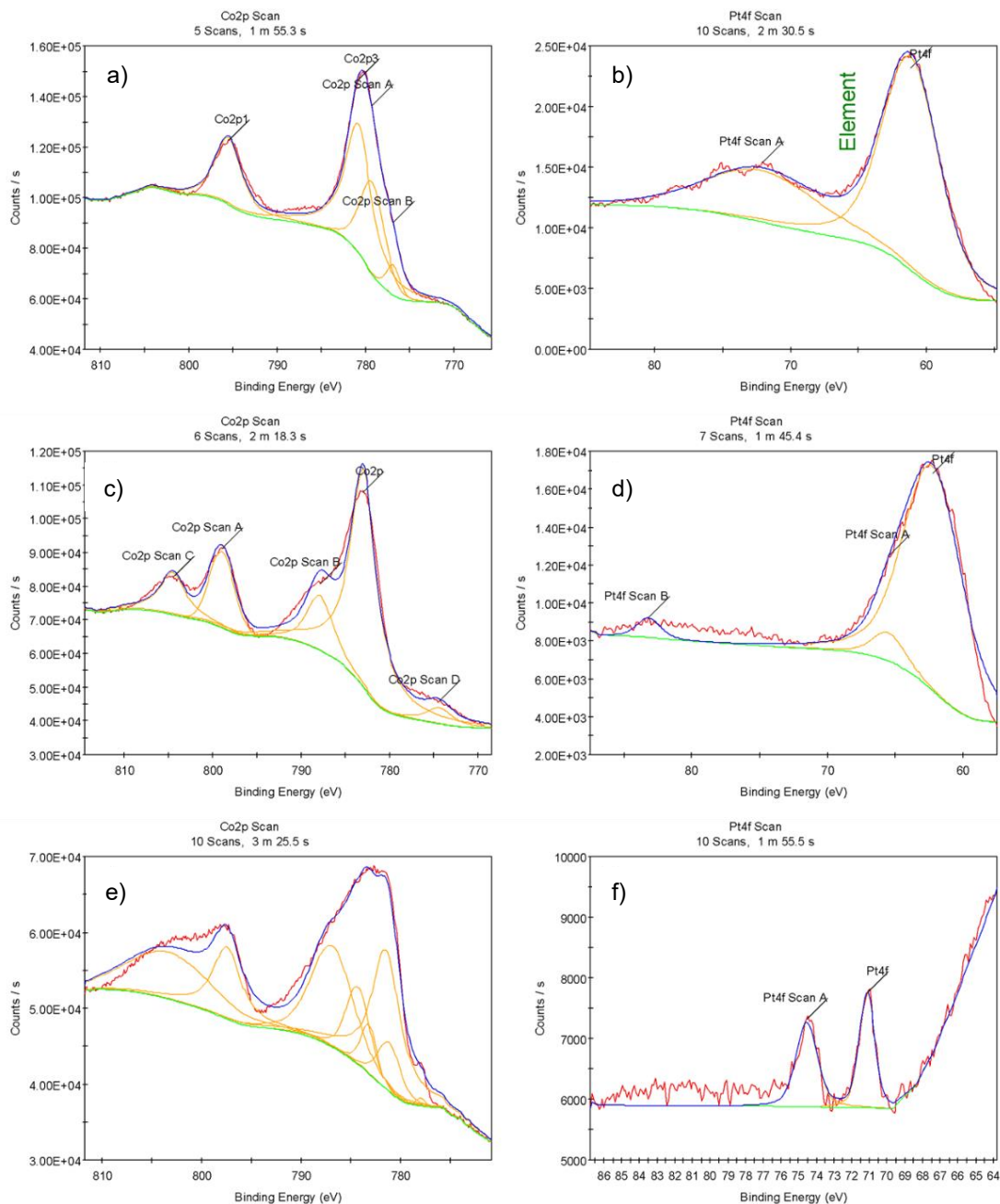
Figure 13. XPS spectra of Co2p and Pt4f orbitals in fresh catalyst (a-b), catalyst after reduction by NaBH₄ (c-d), and catalyst after NO₃⁻N reduction

4.4. Catalyst stability and durability

An important parameter indicating the applicability of the catalyst is its durability and stability in successive reaction cycles. Pt-Co@NC catalyst was tested for NO_3^--N reduction in three reaction cycles without regeneration of catalyst. No reactivation of catalyst by $NaBH_4$ was done between reaction cycles. The results in Figure 14 show that 100% of NO_3^--N reduction was observed in the first two cycles followed by the 96.5% reduction in the third one. The selectivity to NH_4^+-N was 98.3%, 95.8% and 84.9% in all cycles. Reaction rate constant decreased as well. The loss of reactivity of the metallic catalysts is likely attributed to the formation of passivation layer due to interactions with H^+ and water, exposure to oxygen during washing between reaction cycles, agglomeration of metals on the catalyst surface and leaching of metals to the reaction media [101]–[103]. Leaching of Co was analyzed by ICP-OES in all cycles and have shown < 20 ppb indicating negligible Co release to the solution. Similarly, Pt was not detected in all samples indicating no metal leaching during first three cycles of catalytic reduction.
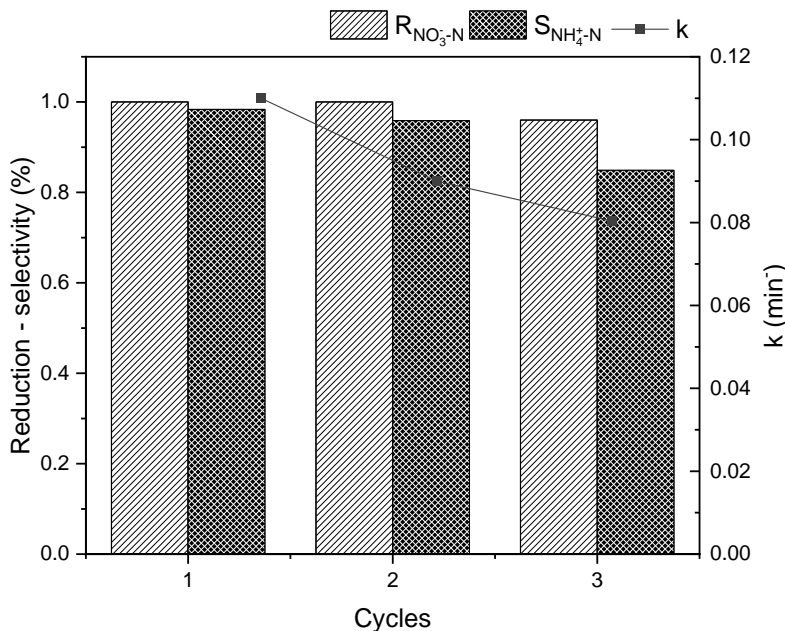
Figure 14. Durability of Pt-Co@NC in repeated reaction cycles without catalyst regeneration.

Chapter 5 – Conclusion

In this work, Pt-Co@NC catalyst derived by carbonization of ZIF-67 was applied to reduce NO_3^- in aqueous media. The catalytic performance was analyzed under varied conditions. Compared to other catalysts reported in the literature, Pt-Co@NC showed competitiveness, demonstrating one of the highest rate constants for the reaction at similar conditions. Overall, the following conclusions could be made:

1. Carbonization of ZIF-67 results in the loss of organic ligands exposing Co to the surface and a reduction in the particle size by approximately 1.2 times. XRD and FTIR confirmed the removal of the major organic functional groups. Impregnation of Pt on the surface of Co@NC led to a decrease on pH_{pzc} from 9.41 to 7.14. The affinity to NO_3^- at pH values below 7.14 are beneficial for nitrate reduction.

2. Under H_2 and CO_2 flow, Co@NC alone has not shown reactivity towards NO_3^- removal, as well as ZIF-67 and homogeneous reduction by $NaBH_4$. Addition of 3.6%wt Pt on the Co@NC surface resulted in enhanced reactivity (11.4×10^{-2} min^{-1}) with the full reduction of 60 mg/L NO_3^-–N in 30 min. 99.5% of NH_4^+ selectivity was observed after desorption.

3. Pt showed the highest reactivity among different metals, while Pd-Co@NC removed 91.6% of NO_3^-–N in 60 min. Generally, all metals showed NH_4^+-N selectivity of >86.6%, except for Ru, which demonstrated sorption behavior for nitrate removal.

4. When Pt content increased from 0.5-3.6%, significant improvement in nitrate reduction was observed. An increase in catalyst loading also positively affected the reactivity of the system as well as the reduction in contaminant concentration.

5. Evaluation of pH variations showed that at pH values lower than pH_{pzc} 100% of nitrate reduction is observed. Selectivity towards NH_4^+-N decreased with an increase in pH.

6. Durability and stability analysis of the catalyst in 3 successive reaction cycles without regeneration showed high catalyst durability. No significant cobalt leaching was observed during all reaction cycles.

Finally, the ZIF-67-derived Co-containing catalyst with Pt impregnated on the surface showed an outstanding reactivity towards nitrate reduction. This is a promising catalyst to test under real-life applications. However, a more in-depth study of the reduction mechanism and role of Co should be performed and evaluation of the effect of other factors on system performance, such as ZIF-67 carbonization temperature, CO_2 and H_2 flow variations, and use of different buffering systems.

References

[1]   D. Keeney and R. A. Olson, "Sources of nitrate to ground water," *http://dx.doi.org/10.1080/10643388609381748*, vol. 16, no. 3, pp. 257–304, Jan. 2009, doi: 10.1080/10643388609381748.

[2]   L. Ma, L. Hu, X. Feng, and S. Wang, "Nitrate and Nitrite in Health and Disease," vol. 9, no. 5, pp. 938–945, 2018, doi: 10.14336/AD.2017.1207.

[3]   A. Dzumagulov, A. Nicolayenko, and I. Mirkhashimov, "Стандарты и нормы качества вод РК.pdf." Regional ecological center of Central Asia, Almaty, 2009.

[4]   "Об утверждении санитарно-эпидемиологических правил и норм по питьевой воде - ИПС 'Әділет.'" https://adilet.zan.kz/rus/docs/V050003608_ (accessed Mar. 23, 2022).

[5]   "Nitrate and nitrite in Drinking-water. Background document for development of WHO Guidelines for Drinking-water Quality," 2003.

[6]   S. K. M. Huno, E. R. Rene, E. D. Van Hullebusch, and A. P. Annachhatre, "Nitrate removal from groundwater: a review of natural and engineered processes," *Journal of Water Supply: Research and Technology-Aqua*, vol. 67, no. 8, pp. 885–902, Dec. 2018, doi: 10.2166/AQUA.2018.194.

[7]   G. Tokazhanov, E. Ramazanova, S. Hamid, S. Bae, and W. Lee, "Advances in the catalytic reduction of nitrate by metallic catalysts for high efficiency and N2 selectivity: A review," *Chemical Engineering Journal*, vol. 384, no. October 2019, p. 123252, 2020, doi: 10.1016/j.cej.2019.123252.

[8]   C. Wang *et al.*, "New Strategies for Novel MOF-Derived Carbon Materials Based on Nanoarchitectures," *Chem*, vol. 6, no. 1, pp. 19–40, Jan. 2020, doi: 10.1016/J.CHEMPR.2019.09.005.

[9]   P. E. Widdison and T. P. Burt, "Nitrogen Cycle," *Encyclopedia of Ecology, Five-Volume Set*. Academic Press, pp. 2526–2533, Jan. 01, 2008. doi: 10.1016/B978-008045405-4.00750-3.

[10]   M. N. Khan, M. Mobin, Z. K. Abbas, and S. A. Alamri, "Fertilizers and Their Contaminants in Soils, Surface and Groundwater," *Encyclopedia of the Anthropocene*, vol. 1–5, pp. 225–240, Jan. 2018, doi: 10.1016/B978-0-12-809665-9.09888-8.

[11]   "World fertilizer trends and outlook to 2020," Rome, 2017. Accessed: May 04, 2023. [Online]. Available: www.fao.org/publications

[12]   "Производство аммиака, аммиачной селитры и минеральных удобрений | Компания КазАзот." https://www.kazazot.kz/selitra (accessed Mar. 23, 2022).

[13]   C. O. Dimkpa, J. Fugice, U. Singh, and T. D. Lewis, "Development of fertilizers for enhanced nitrogen use efficiency – Trends and perspectives," *Science of the Total Environment*, vol. 731, Aug. 2020, doi: 10.1016/J.SCITOTENV.2020.139113.

[14]   B. Le Lin, A. Sakoda, R. Shibasaki, and M. Suzuki, "A Modelling Approach to Global Nitrate Leaching Caused by Anthropogenic Fertilisation," *Water Res*, vol. 35, no. 8, pp. 1961–1968, Jun. 2001, doi: 10.1016/S0043-1354(00)00484-X.

[15]   C. Cobzaru and V. Inglezakis, "Ion Exchange," *Progress in Filtration and Separation*, pp. 425–498, 2015, doi: 10.1016/B978-0-12-384746-1.00010-0.

[16]   M. J. Brandt, K. M. Johnson, A. J. Elphinston, and D. D. Ratnayaka, "Specialized and Advanced Water Treatment Processes," *Twort's Water Supply*, pp. 407–473, Jan. 2017, doi: 10.1016/B978-0-08-100025-0.00010-7.

[17]   K. Amirsadat, H. Sharififard, and A. lashanizadegan, "Adsorption of nitrate from municipal wastewater by synthesized chitosan/iron/activated carbon of orange peel composite," *Biomass Convers Biorefin*, pp. 1–17, Aug. 2022, doi: 10.1007/S13399-022-03198-2/METRICS.

[18]   A. Gierak and I. Łazarska, "Adsorption of nitrate, nitrite, and ammonium ions on carbon adsorbents," *Adsorption Science and Technology*, vol. 35, no. 7–8, pp. 721–727, Sep. 2017, doi: 10.1177/0263617417708085/ASSET/IMAGES/LARGE/10.1177_0263617417708085-FIG2.JPEG.

[19]   H. Zhou, Y. Tan, W. Gao, Y. Zhang, and Y. Yang, "Selective nitrate removal from aqueous solutions by a hydrotalcite-like absorbent FeMgMn-LDH," *Scientific Reports 2020 10:1*, vol. 10, no. 1, pp. 1–10, Sep. 2020, doi: 10.1038/s41598-020-72845-3.

[20]   H. Sadegh and G. A. M. Ali, "Potential Applications of Nanomaterials in Wastewater Treatment," pp. 51–61, Jun. 2018, doi: 10.4018/978-1-5225-5754-8.CH004.

[21]   L. D. McMullen, "Remediation at the Water Treatment Plant," *Nitrogen in the Environment: Sources, Problems and Management*, pp. 455–460, 2001, doi: 10.1016/B978-044450486-9/50020-0.

[22]   T. Priya, B. K. Mishra, and M. N. V. Prasad, "Physico-chemical techniques for the removal of disinfection by-products precursors from water," *Disinfection By-products in Drinking Water: Detection and Treatment*, pp. 23–58, Jan. 2020, doi: 10.1016/B978-0-08-102977-0.00002-0.

[23]   R. Epsztein, O. Nir, O. Lahav, and M. Green, "Selective nitrate removal from groundwater using a hybrid nanofiltration–reverse osmosis filtration scheme," *Chemical Engineering Journal*, vol. 279, pp. 372–378, Nov. 2015, doi: 10.1016/J.CEJ.2015.05.010.

[24]   "2. Biological Nitrification and Denitrification," vol. 54, pp. 43–53, Jan. 1993, doi: 10.1016/S0166-1116(08)70524-7.

[25]   H. Lu, K. Chandran, and D. Stensel, "Microbial ecology of denitrification in biological wastewater treatment," *Water Res*, vol. 64, pp. 237–254, Nov. 2014, doi: 10.1016/J.WATRES.2014.06.042.

[26]   Max. Appl, "Ammonia : principles and industrial practice," p. 301, 1999, Accessed: Sep. 10, 2022. [Online]. Available: https://www.wiley.com/en-us/Ammonia%3A+Principles+and+Industrial+Practice-p-9783527613885

[27]   W. Jung and Y. J. Hwang, "Material strategies in the electrochemical nitrate reduction reaction to ammonia production," *Mater Chem Front*, vol. 5, no. 18, pp. 6803–6823, Sep. 2021, doi: 10.1039/D1QM00456E.

[28]   H. Shen *et al.*, "Electrochemical ammonia synthesis: Mechanistic understanding and catalyst design," *Chem*, vol. 7, no. 7, pp. 1708–1754, Jul. 2021, doi: 10.1016/J.CHEMPR.2021.01.009.

[29]   R. Zhao *et al.*, "Recent progress in the electrochemical ammonia synthesis under ambient conditions," *EnergyChem*, vol. 1, no. 2, p. 100011, Sep. 2019, doi: 10.1016/J.ENCHEM.2019.100011.

[30]　A. R. Singh, B. A. Rohr, M. J. Statt, J. A. Schwalbe, M. Cargnello, and J. K. Nørskov, "Strategies toward Selective Electrochemical Ammonia Synthesis," *ACS Catal*, vol. 9, no. 9, pp. 8316–8324, Sep. 2019, doi: 10.1021/ACSCATAL.9B02245/SUPPL_FILE/CS9B02245_SI_001.PDF.

[31]　D. W. Green and R. H. Perry, *Perry's Chemical Engineers' Handbook, Eighth Edition*. McGraw-Hill Education, 2008. Accessed: Sep. 10, 2022. [Online]. Available: https://www.accessengineeringlibrary.com/content/book/9780071422949

[32]　J. Li *et al.*, "Efficient Ammonia Electrosynthesis from Nitrate on Strained Ruthenium Nanoclusters," *J Am Chem Soc*, vol. 142, no. 15, pp. 7036–7046, Apr. 2020, doi: 10.1021/JACS.0C00418/ASSET/IMAGES/MEDIUM/JA0C00418_M001.GIF.

[33]　Z. Y. Wu *et al.*, "Electrochemical ammonia synthesis via nitrate reduction on Fe single atom catalyst," *Nature Communications 2021 12:1*, vol. 12, no. 1, pp. 1–10, May 2021, doi: 10.1038/s41467-021-23115-x.

[34]　J. M. McEnaney *et al.*, "Electrolyte engineering for efficient electrochemical nitrate reduction to ammonia on a titanium electrode," *ACS Sustain Chem Eng*, vol. 8, no. 7, pp. 2672–2681, Feb. 2020, doi: 10.1021/ACSSUSCHEMENG.9B05983/ASSET/IMAGES/MEDIUM/SC9B05983_M007.GIF.

[35]　K. Kim *et al.*, "Coupling nitrate capture with ammonia production through bifunctional redox-electrodes," *Nature Communications 2023 14:1*, vol. 14, no. 1, pp. 1–13, Feb. 2023, doi: 10.1038/s41467-023-36318-1.

[36]　I. Katsounaros, M. Dortsiou, and G. Kyriacou, "Electrochemical reduction of nitrate and nitrite in simulated liquid nuclear wastes," *J Hazard Mater*, vol. 171, no. 1–3, pp. 323–327, Nov. 2009, doi: 10.1016/J.JHAZMAT.2009.06.005.

[37]　S. Hamid, S. Bae, W. Lee, M. T. Amin, and A. A. Alazba, "Catalytic Nitrate Removal in Continuous Bimetallic Cu-Pd/Nanoscale Zerovalent Iron System," *Ind Eng Chem Res*, vol. 54, no. 24, pp. 6247–6257, Jun. 2015, doi: 10.1021/ACS.IECR.5B01127/SUPPL_FILE/IE5B01127_SI_001.PDF.

[38]　Y. Liu and J. Wang, "Reduction of nitrate by zero valent iron (ZVI)-based materials: A review," *Science of the Total Environment*, vol. 671, pp. 388–403, Jun. 2019, doi: 10.1016/J.SCITOTENV.2019.03.317.

[39]　S. Bae, J. Jung, and W. Lee, "The effect of pH and zwitterionic buffers on catalytic nitrate reduction by TiO2-supported bimetallic catalyst," *Chemical Engineering Journal*, vol. 232, pp. 327–337, Oct. 2013, doi: 10.1016/J.CEJ.2013.07.099.

[40]　S. Hamid and W. Lee, "Reduction of nitrate in groundwater by hematite supported bimetallic catalyst," *Advances in environmental research*, vol. 5, no. 1, pp. 51–59, Mar. 2016, doi: 10.12989/AER.2016.5.1.051.

[41]　S. Hamid, M. A. Kumar, J. I. Han, H. Kim, and W. Lee, "Nitrate reduction on the surface of bimetallic catalysts supported by nano-crystalline beta-zeolite (NBeta)," *Green Chemistry*, vol. 19, no. 3, pp. 853–866, 2017, doi: 10.1039/c6gc02349e.

[42]　R. A. Crane and T. B. Scott, "Nanoscale zero-valent iron: Future prospects for an emerging water treatment technology," *J Hazard Mater*, vol. 211–212, pp. 112–125, Apr. 2012, doi: 10.1016/J.JHAZMAT.2011.11.073.

[43] N. Ezzatahmadi *et al.*, "Clay-supported nanoscale zero-valent iron composite materials for the remediation of contaminated aqueous solutions: A review," *Chemical Engineering Journal*, vol. 312, pp. 336–350, Mar. 2017, doi: 10.1016/J.CEJ.2016.11.154.

[44] Y. Liu and J. Wang, "Reduction of nitrate by zero valent iron (ZVI)-based materials: A review," *Science of The Total Environment*, vol. 671, pp. 388–403, Jun. 2019, doi: 10.1016/J.SCITOTENV.2019.03.317.

[45] Y. H. Liou, S. L. Lo, C. J. Lin, W. H. Kuan, and S. C. Weng, "Chemical reduction of an unbuffered nitrate solution using catalyzed and uncatalyzed nanoscale iron particles," *J Hazard Mater*, vol. 127, no. 1–3, pp. 102–110, Dec. 2005, doi: 10.1016/J.JHAZMAT.2005.06.029.

[46] S. Bae, S. Hamid, J. Jung, Y. Sihn, and W. Lee, "Effect of promoter and noble metals and suspension pH on catalytic nitrate reduction by bimetallic nanoscale Fe0 catalysts," *http://dx.doi.org/10.1080/09593330.2015.1101166*, vol. 37, no. 9, pp. 1077–1087, May 2015, doi: 10.1080/09593330.2015.1101166.

[47] S. Hamid, S. Bae, W. Lee, M. T. Amin, and A. A. Alazba, "Catalytic Nitrate Removal in Continuous Bimetallic Cu-Pd/Nanoscale Zerovalent Iron System," *Ind Eng Chem Res*, vol. 54, no. 24, pp. 6247–6257, Jun. 2015, doi: 10.1021/ACS.IECR.5B01127/SUPPL_FILE/IE5B01127_SI_001.PDF.

[48] G. M. Curcio, C. Limonti, A. Siciliano, and I. Kabdaşlı, "Nitrate Removal by Zero-Valent Metals: A Comprehensive Review," *Sustainability 2022, Vol. 14, Page 4500*, vol. 14, no. 8, p. 4500, Apr. 2022, doi: 10.3390/SU14084500.

[49] A. P. Murphy, "Chemical removal of nitrate from water," *Nature 1991 350:6315*, vol. 350, no. 6315, pp. 223–225, 1991, doi: 10.1038/350223a0.

[50] G. K. Luk and W. C. Au-Yeung, "Experimental investigation on the chemical reduction of nitrate from groundwater," *Advances in Environmental Research*, vol. 6, no. 4, pp. 441–453, Oct. 2002, doi: 10.1016/S1093-0191(01)00072-7.

[51] A. Siciliano, G. M. Curcio, and C. Limonti, "Chemical Denitrification with Mg0 Particles in Column Systems," *Sustainability 2020, Vol. 12, Page 2984*, vol. 12, no. 7, p. 2984, Apr. 2020, doi: 10.3390/SU12072984.

[52] A. Siciliano, G. M. Curcio, and C. Limonti, "Experimental Analysis and Modeling of Nitrate Removal through Zero-Valent Magnesium Particles," *Water 2019, Vol. 11, Page 1276*, vol. 11, no. 6, p. 1276, Jun. 2019, doi: 10.3390/W11061276.

[53] M. Kumar and S. Chakraborty, "Chemical denitrification of water by zero-valent magnesium powder," *J Hazard Mater*, vol. 135, no. 1–3, pp. 112–121, Jul. 2006, doi: 10.1016/J.JHAZMAT.2005.11.031.

[54] T. H. Jeon, Z. Y. Wu, F. Y. Chen, W. Choi, P. J. J. Alvarez, and H. Wang, "Cobalt-Copper Nanoparticles on Three-Dimensional Substrate for Efficient Ammonia Synthesis via Electrocatalytic Nitrate Reduction," *Journal of Physical Chemistry C*, vol. 126, no. 16, pp. 6982–6989, Apr. 2022, doi: 10.1021/ACS.JPCC.1C10781/ASSET/IMAGES/LARGE/JP1C10781_0004.JPEG.

[55] W. He *et al.*, "Splicing the active phases of copper/cobalt-based catalysts achieves high-rate tandem electroreduction of nitrate to ammonia," *Nature Communications 2022 13:1*, vol. 13, no. 1, pp. 1–13, Mar. 2022, doi: 10.1038/s41467-022-28728-4.
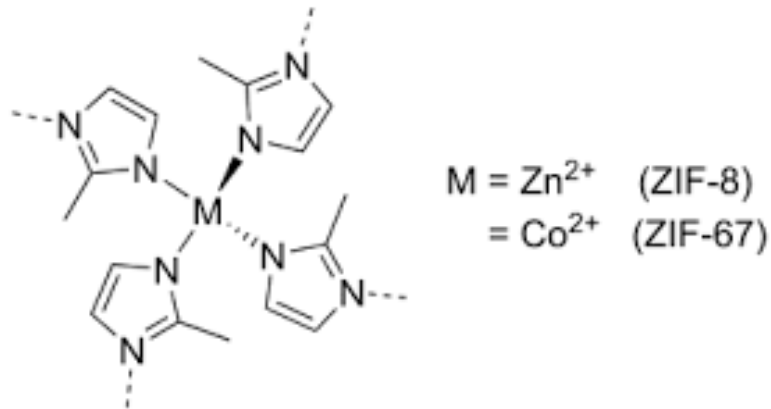
[56]   Y. Guo, J. R. Stroka, B. Kandemir, C. E. Dickerson, and K. L. Bren, "Cobalt Metallopeptide Electrocatalyst for the Selective Reduction of Nitrite to Ammonium," *J Am Chem Soc*, vol. 140, no. 49, pp. 16888–16892, Dec. 2018, doi: 10.1021/JACS.8B09612/ASSET/IMAGES/LARGE/JA-2018-09612X_0005.JPEG.

[57]   O. Q. Carvalho *et al.*, "Role of Electronic Structure on Nitrate Reduction to Ammonium: A Periodic Journey," *J Am Chem Soc*, vol. 144, no. 32, pp. 14809–14818, Aug. 2022, doi: 10.1021/JACS.2C05673/ASSET/IMAGES/LARGE/JA2C05673_0008.JPEG.

[58]   S. Jung, S. Bae, and W. Lee, "Development of Pd-Cu/hematite catalyst for selective nitrate reduction," *Environ Sci Technol*, vol. 48, no. 16, pp. 9651–9658, Aug. 2014, doi: 10.1021/ES502263P/SUPPL_FILE/ES502263P_SI_001.PDF.

[59]   S. Hamid, S. Bae, and W. Lee, "Novel bimetallic catalyst supported by red mud for enhanced nitrate reduction," *Chemical Engineering Journal*, vol. 348, pp. 877–887, Sep. 2018, doi: 10.1016/J.CEJ.2018.05.016.

[60]   H. García and S. Navalon, "Metal-Organic Frameworks : Applications in Separations and Catalysis".

[61]   J. Fonseca, T. Gong, L. Jiao, and H. L. Jiang, "Metal–organic frameworks (MOFs) beyond crystallinity: amorphous MOFs, MOF liquids and MOF glasses," *J Mater Chem A Mater*, vol. 9, no. 17, pp. 10562–10611, May 2021, doi: 10.1039/D1TA01043C.

[62]   H. Fan, M. Peng, I. Strauss, A. Mundstock, H. Meng, and J. Caro, "MOF-in-COF molecular sieving membrane for selective hydrogen separation," *Nature Communications 2021 12:1*, vol. 12, no. 1, pp. 1–10, Jan. 2021, doi: 10.1038/s41467-020-20298-7.

[63]   R. Freund *et al.*, "The Current Status of MOF and COF Applications," *Angewandte Chemie International Edition*, vol. 60, no. 45, pp. 23975–24001, Nov. 2021, doi: 10.1002/ANIE.202106259.

[64]   J. Lee, O. K. Farha, J. Roberts, K. A. Scheidt, S. T. Nguyen, and J. T. Hupp, "Metal-organic framework materials as catalysts," *Chem Soc Rev*, vol. 38, no. 5, pp. 1450–1459, 2009, doi: 10.1039/b807080f.

[65]   J. Sánchez-Laínez *et al.*, "Synthesis of ZIF-93/11 Hybrid Nanoparticles via Post-Synthetic Modification of ZIF-93 and Their Use for H2/CO2 Separation," *Chemistry - A European Journal*, vol. 24, no. 43, pp. 11211–11219, Aug. 2018, doi: 10.1002/CHEM.201802124.

[66]   M. Bergaoui, M. Khalfaoui, A. Awadallah-F, and S. Al-Muhtaseb, "A review of the features and applications of ZIF-8 and its derivatives for separating CO2 and isomers of C3- and C4-hydrocarbons," *J Nat Gas Sci Eng*, vol. 96, p. 104289, Dec. 2021, doi: 10.1016/J.JNGSE.2021.104289.

[67]   B. Chen, Z. Yang, Y. Zhu, and Y. Xia, "Zeolitic imidazolate framework materials: recent progress in synthesis and applications," *J Mater Chem A Mater*, vol. 2, no. 40, pp. 16811–16831, Sep. 2014, doi: 10.1039/C4TA02984D.

[68]   H. S. Jadhav, H. A. Bandal, S. Ramakrishna, and H. Kim, "Critical Review, Recent Updates on Zeolitic Imidazolate Framework-67 (ZIF-67) and Its Derivatives for Electrochemical Water Splitting," *Advanced Materials*, vol. 34, no. 11, p. 2107072, Mar. 2022, doi: 10.1002/ADMA.202107072.

[69]   B. Chen, Z. Yang, Y. Zhu, and Y. Xia, "Zeolitic imidazolate framework materials: recent progress in synthesis and applications," *J Mater Chem A Mater*, vol. 2, no. 40, pp. 16811–16831, Sep. 2014, doi: 10.1039/C4TA02984D.

[70]   M. Mon, R. Bruno, J. Ferrando-Soria, D. Armentano, and E. Pardo, "Metal–organic framework technologies for water remediation: towards a sustainable ecosystem," *J Mater Chem A Mater*, vol. 6, no. 12, pp. 4912–4947, Mar. 2018, doi: 10.1039/C8TA00264A.

[71]   J. Sun, W. Gao, H. Fei, and G. Zhao, "Efficient and selective electrochemical reduction of nitrate to N2 by relay catalytic effects of Fe-Ni bimetallic sites on MOF-derived structure," *Appl Catal B*, vol. 301, p. 120829, Feb. 2022, doi: 10.1016/J.APCATB.2021.120829.

[72]   H. Choi *et al.*, "Vapor-Phase Fabrication and Condensed-Phase Application of a MOF-Node-Supported Iron Thiolate Photocatalyst for Nitrate Conversion to Ammonium," *ACS Appl Energy Mater*, vol. 2, no. 12, pp. 8695–8700, 2019, doi: 10.1021/acsaem.9b01664.

[73]   J. Qin *et al.*, "Achieving high selectivity for nitrate electrochemical reduction to ammonia over MOF-supported RuxOy clusters," *J Mater Chem A Mater*, vol. 10, no. 8, pp. 3963–3969, Feb. 2022, doi: 10.1039/D1TA09441F.

[74]   S. Yuan *et al.*, "Stable Metal–Organic Frameworks: Design, Synthesis, and Applications," *Advanced Materials*, vol. 30, no. 37, p. 1704303, Sep. 2018, doi: 10.1002/ADMA.201704303.

[75]   S. Gao *et al.*, "Improving the Acidic Stability of Zeolitic Imidazolate Frameworks by Biofunctional Molecules," *Chem*, vol. 5, no. 6, pp. 1597–1608, Jun. 2019, doi: 10.1016/J.CHEMPR.2019.03.025.

[76]   H. Zhang, M. Zhao, and Y. S. Lin, "Stability of ZIF-8 in water under ambient conditions," *Microporous and Mesoporous Materials*, vol. 279, pp. 201–210, May 2019, doi: 10.1016/J.MICROMESO.2018.12.035.

[77]   C. Wang, X. Liu, N. Keser Demir, J. P. Chen, and K. Li, "Applications of water stable metal–organic frameworks," *Chem Soc Rev*, vol. 45, no. 18, pp. 5107–5134, Sep. 2016, doi: 10.1039/C6CS00362A.

[78]   C. Hu *et al.*, "Porosity-Induced High Selectivity for CO2 Electroreduction to CO on Fe-Doped ZIF-Derived Carbon Catalysts," *ACS Catal*, vol. 9, no. 12, pp. 11579–11588, Dec. 2019, doi: 10.1021/ACSCATAL.9B03175/SUPPL_FILE/CS9B03175_SI_001.PDF.

[79]   Y. Xiao, H. Yang, X. Bu, and P. Feng, "ZIF-8 derived carbon materials with multifunctional selective adsorption abilities," *Carbon N Y*, vol. 176, pp. 421–430, May 2021, doi: 10.1016/J.CARBON.2021.02.043.

[80]   D. Saliba, M. Ammar, M. Rammal, M. Al-Ghoul, and M. Hmadeh, "Crystal Growth of ZIF-8, ZIF-67, and Their Mixed-Metal Derivatives," *J Am Chem Soc*, vol. 140, no. 5, pp. 1812–1823, Feb. 2018, doi: 10.1021/JACS.7B11589/SUPPL_FILE/JA7B11589_SI_002.MOV.

[81]   J. R. A. Sietsma, A. Jos van Dillen, P. E. de Jongh, and K. P. de Jong, "Application of ordered mesoporous materials as model supports to study catalyst preparation by impregnation and drying," *Stud Surf Sci Catal*, vol. 162, pp. 95–102, Jan. 2006, doi: 10.1016/S0167-2991(06)80895-5.

[82]   S. Hamid, M. A. Kumar, and W. Lee, "Highly reactive and selective Sn-Pd bimetallic catalyst supported by nanocrystalline ZSM-5 for aqueous nitrate reduction," *Appl Catal B*, vol. 187, pp. 37–46, Jun. 2016, doi: 10.1016/J.APCATB.2016.01.035.

[83]   J. Qian, F. Sun, and L. Qin, "Hydrothermal synthesis of zeolitic imidazolate framework-67 (ZIF-67) nanocrystals," *Mater Lett*, vol. 82, pp. 220–223, Sep. 2012, doi: 10.1016/J.MATLET.2012.05.077.
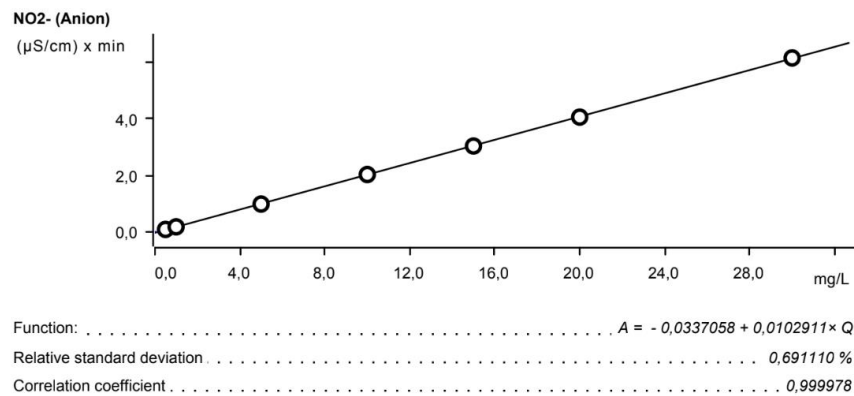
[84]   S. Su *et al.*, "Zeolitic Imidazolate Framework-67: A promising candidate for recovery of uranium (VI) from seawater," *Colloids Surf A Physicochem Eng Asp*, vol. 547, pp. 73–80, Jun. 2018, doi: 10.1016/J.COLSURFA.2018.03.042.

[85]   A. M. Mohamed, W. A. Abbas, G. E. Khedr, W. Abass, and N. K. Allam, "Computational and experimental elucidation of the boosted stability and antibacterial activity of ZIF-67 upon optimized encapsulation with polyoxometalates," *Scientific Reports 2022 12:1*, vol. 12, no. 1, pp. 1–10, Sep. 2022, doi: 10.1038/s41598-022-20392-4.

[86]   K. Archana, N. G. Pillai, K. Y. Rhee, and A. Asif, "Super paramagnetic ZIF-67 metal organic framework nanocomposite," *Compos B Eng*, vol. 158, pp. 384–389, Feb. 2019, doi: 10.1016/J.COMPOSITESB.2018.10.005.

[87]   M. Ammar, S. Jiang, and S. Ji, "Heteropoly acid encapsulated into zeolite imidazolate framework (ZIF-67) cage as an efficient heterogeneous catalyst for Friedel-Crafts acylation," *J Solid State Chem*, vol. 233, pp. 303–310, Jan. 2016, doi: 10.1016/J.JSSC.2015.11.014.

[88]   H. Wang *et al.*, "Core-Shell ZIF67@ZIF8 Modified with Phytic Acid as an Effective Flame Retardant for Improving the Fire Safety of Epoxy Resins," *ACS Omega*, vol. 7, no. 25, pp. 21664–21674, Jun. 2022, doi: 10.1021/ACSOMEGA.2C01545/ASSET/IMAGES/LARGE/AO2C01545_0014.JPEG.

[89]   J. Tang *et al.*, "Electrochemical determination of dopamine and uric acid using a glassy carbon electrode modified with a composite consisting of a Co(II)-based metalorganic framework (ZIF-67) and graphene oxide," *Microchimica Acta*, vol. 185, no. 10, pp. 1–11, Oct. 2018, doi: 10.1007/S00604-018-3025-X/METRICS.

[90]   Y. Sakamoto, Y. Kamiya, and T. Okuhara, "Selective hydrogenation of nitrate to nitrite in water over Cu-Pd bimetallic clusters supported on active carbon," *J Mol Catal A Chem*, vol. 250, no. 1–2, pp. 80–86, May 2006, doi: 10.1016/J.MOLCATA.2006.01.041.

[91]   S. Hamid, M. A. Kumar, J. I. Han, H. Kim, and W. Lee, "Nitrate reduction on the surface of bimetallic catalysts supported by nano-crystalline beta-zeolite (NBeta)," *Green Chemistry*, vol. 19, no. 3, pp. 853–866, Feb. 2017, doi: 10.1039/C6GC02349E.

[92]   O. S. G. P. Soares, J. J. M. Órfão, and M. F. R. Pereira, "Bimetallic catalysts supported on activated carbon for the nitrate reduction in water: Optimization of catalysts composition," *Appl Catal B*, vol. 91, no. 1–2, pp. 441–448, Sep. 2009, doi: 10.1016/J.APCATB.2009.06.013.

[93]   O. S. G. P. Soares, J. J. M. Órfão, and M. F. R. Pereira, "Nitrate reduction in water catalysed by Pd-Cu on different supports," *Desalination*, vol. 279, no. 1–3, pp. 367–374, Sep. 2011, doi: 10.1016/J.DESAL.2011.06.037.

[94]   W. Zhao, X. Zhu, Y. Wang, Z. Ai, and D. Zhao, "Catalytic reduction of aqueous nitrates by metal supported catalysts on Al particles," *Chemical Engineering Journal*, vol. 254, pp. 410–417, Oct. 2014, doi: 10.1016/J.CEJ.2014.05.144.

[95]   S. Mossa Hosseini, B. Ataie-Ashtiani, and M. Kholghi, "Nitrate reduction by nano-Fe/Cu particles in packed column," *Desalination*, vol. 276, no. 1–3, pp. 214–221, Aug. 2011, doi: 10.1016/J.DESAL.2011.03.051.

[96]   Y. H. Liou, S. L. Lo, C. J. Lin, W. H. Kuan, and S. C. Weng, "Chemical reduction of an unbuffered nitrate solution using catalyzed and uncatalyzed nanoscale iron particles," *J Hazard Mater*, vol. 127, no. 1–3, pp. 102–110, Dec. 2005, doi: 10.1016/J.JHAZMAT.2005.06.029.

[97]   S. Guo *et al.*, "Insights into Nitrate Reduction over Indium-Decorated Palladium Nanoparticle Catalysts," *ACS Catal*, vol. 8, no. 1, pp. 503–515, Jan. 2018, doi: 10.1021/ACSCATAL.7B01371/ASSET/IMAGES/MEDIUM/CS-2017-01371P_0014.GIF.

[98]   S. Hamid, S. Bae, W. Lee, M. T. Amin, and A. A. Alazba, "Catalytic Nitrate Removal in Continuous Bimetallic Cu-Pd/Nanoscale Zerovalent Iron System," *Ind Eng Chem Res*, vol. 54, no. 24, pp. 6247–6257, Jun. 2015, doi: 10.1021/ACS.IECR.5B01127/SUPPL_FILE/IE5B01127_SI_001.PDF.

[99]   Y. Zeng, H. Walker, and Q. Zhu, "Reduction of nitrate by NaY zeolite supported Fe, Cu/Fe and Mn/Fe nanoparticles," *J Hazard Mater*, vol. 324, pp. 605–616, Feb. 2017, doi: 10.1016/J.JHAZMAT.2016.11.032.

[100]   Y. X. Chen, Y. Zhang, and G. H. Chen, "Appropriate conditions or maximizing catalytic reduction efficiency of nitrate into nitrogen gas in groundwater," *Water Res*, vol. 37, no. 10, pp. 2489–2495, May 2003, doi: 10.1016/S0043-1354(03)00028-9.

[101]   S. Bae, S. Hamid, J. Jung, Y. Sihn, and W. Lee, "Effect of promoter and noble metals and suspension pH on catalytic nitrate reduction by bimetallic nanoscale Fe0 catalysts," *http://dx.doi.org/10.1080/09593330.2015.1101166*, vol. 37, no. 9, pp. 1077–1087, May 2015, doi: 10.1080/09593330.2015.1101166.

[102]   J. Jung, S. Bae, and W. Lee, "Nitrate reduction by maghemite supported Cu-Pd bimetallic catalyst," *Appl Catal B*, vol. 127, pp. 148–158, Oct. 2012, doi: 10.1016/J.APCATB.2012.08.017.

[103]   W. Zhao, X. Zhu, Y. Wang, Z. Ai, and D. Zhao, "Catalytic reduction of aqueous nitrates by metal supported catalysts on Al particles," *Chemical Engineering Journal*, vol. 254, pp. 410–417, Oct. 2014, doi: 10.1016/J.CEJ.2014.05.144.

[104]   C. Dietrich *et al.*, "The relation between crystal structure and the occurrence of quantum-rotor-induced polarization," *Magnetic Resonance*, vol. 2, no. 2, pp. 751–763, 2021, doi: 10.5194/MR-2-751-2021.
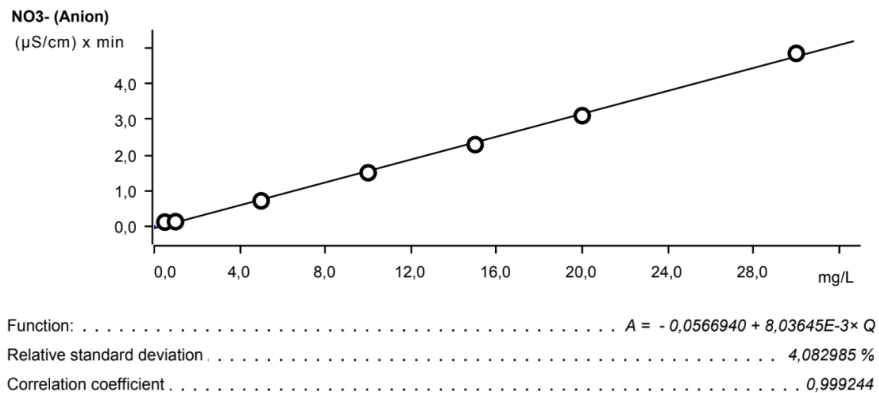
Appendix

Figure A 1. The structure of ZIF-8 and ZIF-67 [104].

Function: . . . . $A = -0,0337058 + 0,0102911 \times Q$

Relative standard deviation . . . . *0,691110 %*

Correlation coefficient *0,999978*

Figure A 2. IC calibration curve for NO_2^- in a range of 0-30 mg/l

Function: . . . . $A = -0,0566940 + 8,03645E\text{-}3 \times Q$

Relative standard deviation . . . . *4,082985 %*

Correlation coefficient *0,999244*

Figure A 3. IC calibration curve for NO_3^- in a range of 0-30 mg/l

NH4+ (Cation)

Function: . . . . $A = -0,0165087 + 0,0156081 \times Q + 1,97516E\text{-}7 \times Q^2$

Relative standard deviation . . . . *1,650584 %*

Correlation coefficient *0,999915*
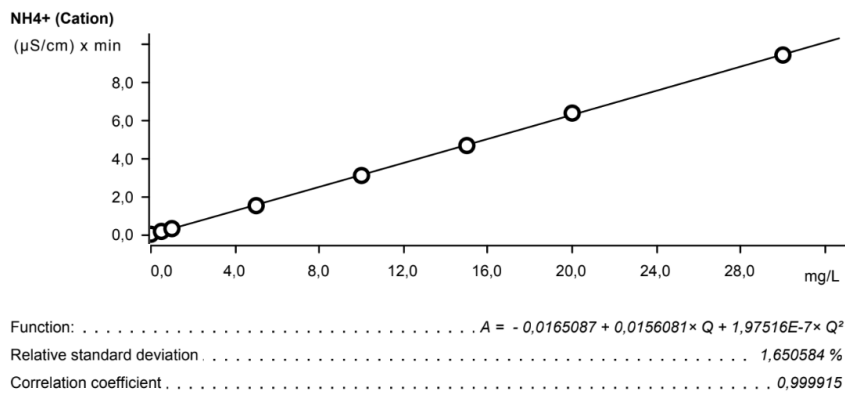
Figure A 4. IC calibration curve for NH₄⁺ in a range of 0-30 mg/l

Na+ (Cation)

Function: . . . . $A = -0,0113944 + 0,0135670 \times Q + 1,68328E\text{-}7 \times Q^2$

Relative standard deviation . . . . *1,712759 %*

Correlation coefficient *0,999908*
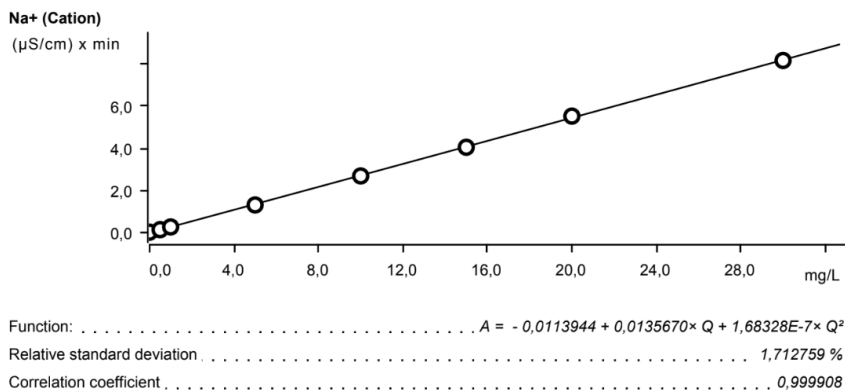
Figure A 5. IC calibration curve for Na⁺ in a range of 0-30 mg/l
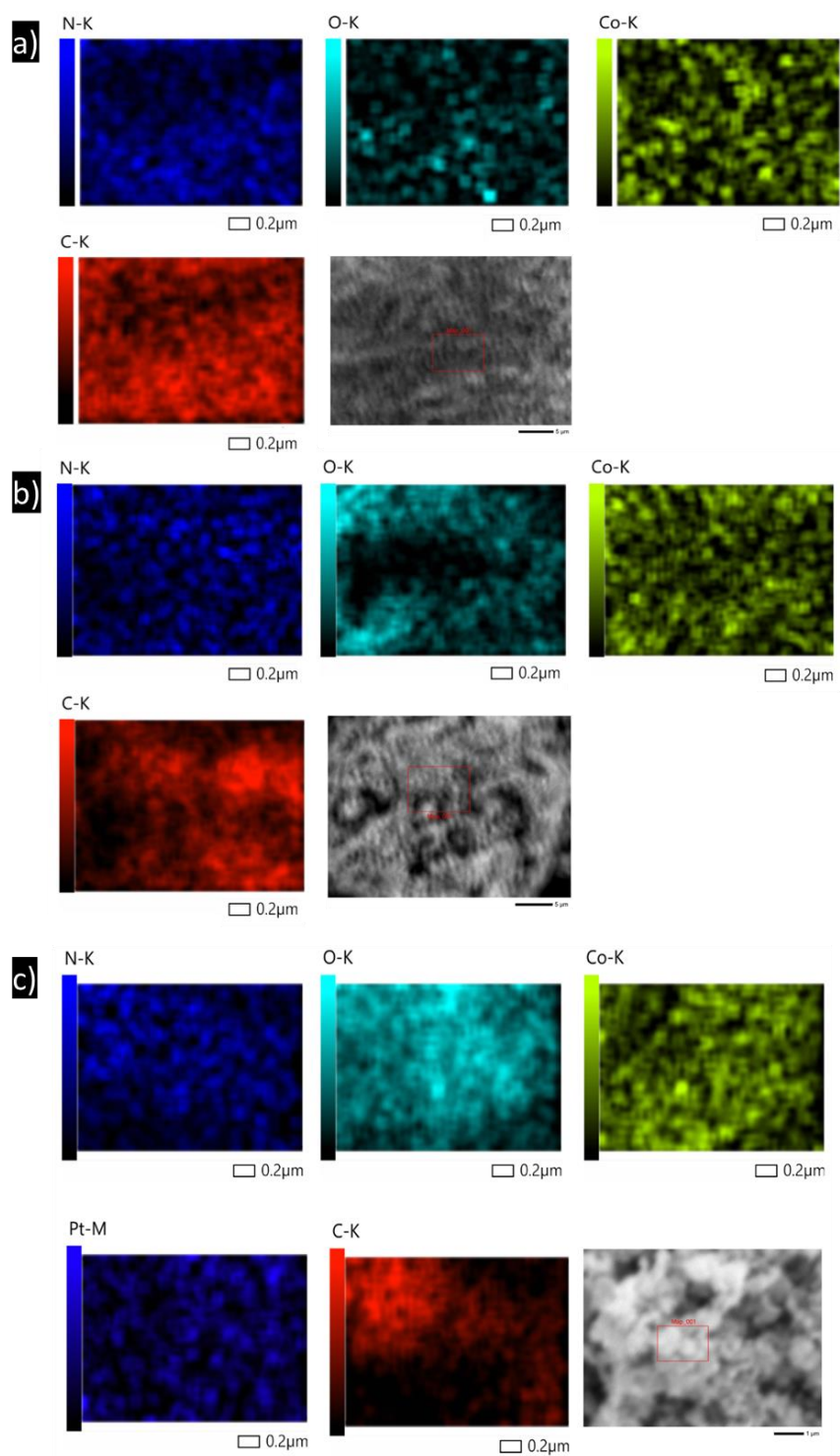
Figure A 6. SEM-EDS Elemental mapping of ZIF-67 (a), Co@NC (b), and Pt-Co@NC (c).